TECTONICS, VOL. 14, NO. 3, PAGES 658-676 , JUNE 1995

Activation of the Nyainqentanghla Shear Zone: Implications for uplift of the southern Tibetan Plateau

T. Mark Harrison,[1] Peter Copeland,[2] W.S.F. Kidd,[3] and Oscar M. Lovera[1]

Abstract. Neogene extension of the Tibetan plateau is manifested as a series of north-south trending graben, the most prominent of which is the Yadong-Gulu rift. The Nyainqentanghla Shan, a NE-SW trending mountain range ~100 km NW of Lhasa, bounds the western margin of the Yangbajian graben, the central segment of the Yadong-Gulu rift. The eastern edge of the Nyainqentanghla massif is marked by a low angle (~25°) detachment fault shear zone of amphibolite grade mylonites. The $^{40}Ar/^{39}Ar$ thermal history results from samples collected along two deeply incised valleys within the massif reveal that a rapid cooling event propagated from ~8 Ma in the core of the range to ~4 Ma within the high strain zone at the eastern boundary. Assuming that faulting initiated at high angle (~60°), thermal histories were fit to a numerical simulation of slip on a normal fault to yield estimates of both the age of fault initiation and the slip rate history. The form of the isotopically derived thermal histories are similar to general form predicted by the thermal model and suggests that significant movement began at 8±1 Ma in the southern valley (Goring-la) and proceeded at an average slip rate of ~3 mm/yr between ~8 and 3 Ma. A more complex history is required to fit the data from the northern valley (Balum Chun), but the timing of initiation and average slip rate are similar to the Goring-la result. Numerical simulations in which the fault angle is varied indicate that the isotopically derived temperature histories are inconsistent with slip occurring at low angle (<40°). Because the extension direction of the Yangbajian graben is representative of most rifts on the southern Tibetan plateau, our data suggest that crustal thickness and elevation reached close to their present values by 8±1 Ma. A carbon isotopic shift in pedogenic carbonates from the Siwalik Formation at about 7.5 Ma appears to reflect intensification of the Asian monsoon and, by inference, that the plateau had attained an important threshold elevation by that time. Formation of a diffuse plate boundary in the Indian oceanic lithosphere beginning at 7.5-8.0 Ma is also consistent with this history. We suggest that the plateau had attained a threshold area and elevation by 8±1 Ma sufficient to trigger these three independent manifestations.

[1]Department of Earth and Space Sciences and Institute of Geophysics and Planetary Physics, University of California, Los Angeles.

[2]Department of Geosciences, University of Houston, Houston, Texas.

[3]Department of Geological Sciences, State University of New York at Albany, Albany, New York.

Paper number 95TC00608.
0278-7407/95/95TC-00608$10.00

Introduction

Since the beginning of the Indo-Eurasian collision at about 50 Ma, convergence within Asia has been accommodated in the upper crust by several mechanisms: large-scale thrusting in the Himalaya [e.g., *Le Fort, 1989*] and southern [e.g., *Yin et al.*, 1994] and central Tibet [e.g., *Chang et al.*, 1986]; major strike-slip faulting, both on the margin and within the Tibetan plateau [e.g., *Tapponnier and Molnar*, 1976; *Tapponnier et al.*, 1986]; and E-W extension on the southern Tibetan plateau [e.g., *Armijo et al.*, 1986]. This extension has been accommodated by a series of generally N-S trending rift valleys throughout southern Tibet (Figure 1). Development of these graben marks a significant shift in the state of stress within the Tibetan crust, and determining the timing of these features would be an important step in understanding the evolution of the plateau. There is general agreement that this extension reflects orogenic collapse following attainment of maximum sustainable elevation for the conditions extant in southern Tibet [e.g., *Tapponnier et al.*, 1986; *England and Houseman*, 1989; *Dewey*, 1988]. Stratigraphic and geomorphological relationships indicate that the graben-defining normal faults have been active in southern Tibet throughout the Pleistocene [*Armijo et al.*, 1986], but do not permit their upper age limit to be precisely defined. This paper presents thermochronological data from the uplifted footwall of a major detachment system on the southern Tibetan plateau which appears to reflect the timing of graben formation.

The Nyainqentanghla is a NE-SW trending mountain range of unusually prominent relief in southern Tibet, located approximately 100 km NW of Lhasa (Figure 2a). The Nyainqentanghla bounds the western margin of the Yangbajian graben (Figure 3), a segment of the Yadong-Gulu rift [*Armijo et al.*, 1986; *Pan and Kidd*, 1992]. The Yadong-Gulu rift, the most prominent graben system in southern Tibet, is unusual in that although most Quaternary graben in southern Tibet strike N-S, the central portion of this rift strikes NE-SW (Figure 1), likely controlled by preexisting structures in the Nyainqentanghla basement [*Armijo et al.*, 1986]. Within the framework of the orogenic collapse hypothesis, the time of normal fault initiation marks the attainment of maximum elevation of the southern Tibetan plateau. Knowing when the Tibetan plateau reached its present size and elevation has implications not only to geodynamics but also to global atmospheric circulation, the onset of the Asian monsoon, and factors controlling ecological evolution in Asia. Alternatively, the range could originate as a wedge extrusion feature that transfers strike-slip motion from the Tsangpo suture zone to the Karakorum-Jiali fault zone [*Armijo et al.*, 1989; *Tapponnier*, 1993]. In this view, the Nyainqentanghla detachment fault is the extensional compliment of a postulated SE dipping, NW directed thrust fault bounding the NW side of the range [*Kidd et al.*, 1988].

The rocks exposed in the Nyainqentanghla are a diverse assemblage dominated by biotite granite, granitoid gneiss, and

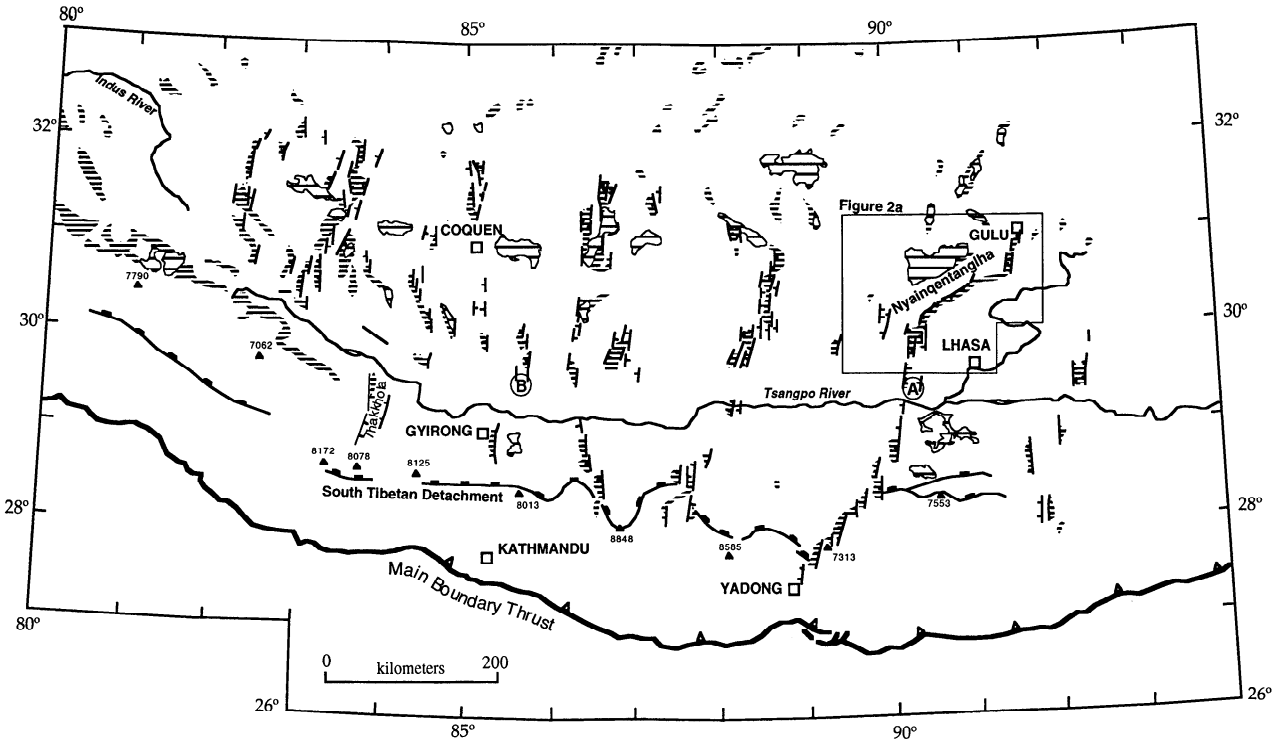

Figure 1. Map showing the major N-S trending normal faults and rift basins of southern Tibet (Modified from *Armijo et al.* [1986]). Normal faults are marked by thick solid lines with the dip direction indicated by the orthogonal ticks. Graben fill is represented by closely spaced horizontal lines. Lakes are shown as outlined regions with thick horizontal lines. The suture separating rocks of Indian affinity from the Lhasa block is approximately located along the course of the Tsangpo River. Locations indicated by the circled letters A and B are for basement samples XR-2a and CH-30, respectively. These rocks experienced rapid cooling, possibly due to tectonic denudation, at 8 Ma. The region shown in Figure 2a is outlined by a polygon.

pelitic schists; minor rock types include pyroxenite and amphibolite. In the northeast part of the range, phyllites are the dominant rock type with subordinate schists. Previous geochronologic investigations suggest that the ages of formation of the gneisses within the Nyainqentanghla are dominantly Cretaceous and late Paleozoic [*Xu et al.*, 1985]. Reconnaissance geochronology of one of the biotite granites indicates a crystallization age of about 50 Ma [*Xu et al.*, 1985]. Metamorphic assemblages from rocks within and adjacent to the northeastern part of the range indicate peak conditions of ~5 kbar and 600-700°C [*Harris et al.*, 1988]. Extension within the graben continues to the present day [*Armijo et al.*, 1986]. Peaks in the range reach elevations in excess of 7000 m, and the valleys surrounding the range are at elevations from 4000 to 4500 m. Alpine glaciers and ice fields cover much of the range above 6500 m (Figure 2a). At the southern edge of the range, the Nyainqentanghla is juxtaposed along a fault contact with the Linzizong Group, a series of andesitic to rhyolitic ignimbrites thought to be coeval with the batholith of the Gangdese Shan [*Copeland et al.*, 1995].

Traverses were made through two deeply incised hanging valleys in the central portion of the range: the Goring-la in the south and the Balum Chun about 15 km to the NW (Figure 2b). Outcrops on the southern and north-eastern rims of the Nyainqentanghla were also sampled (Figure 2a). Seventeen samples were analyzed for $^{40}Ar/^{39}Ar$; three from the southernmost part of the range, ten from the central part of the range, and four from the northern part of the range. Apatite fission track ages have been previously measured from four samples; one from the southern, two from the central, and one from the northern parts of the range [*Pan et al.*, 1993].

Thermochronological Results

Analytical methods for $^{40}Ar/^{39}Ar$ followed the procedures outlined by *Harrison et al.* [1991]. All uncertainties are quoted at 1σ. The $^{40}Ar/^{39}Ar$ analyses were performed on either a Nuclide 4.5-60-RSS mass spectrometer, or a VG1200S mass spectrometer and results are either held in radon.css.ucla.edu (128.97.31.46) in directory pub/tables/nqtl (and can be obtained directly from the anonymous account via ftp) or are given by *Copeland* [1990].

The $^{40}Ar/^{39}Ar$ K-feldspar data of selected samples were interpreted using the multidiffusion domain model [*Lovera et al.*, 1989, 1991; *Harrison et al.*, 1991; *Richter et al.*, 1991]. This approach models the form of the Arrhenius plot and age spectrum as a function of the diffusion domain parameters (radius of diffusion domain, ρ, volume fraction of each domain, ϕ, activation energy, E, and frequency factor, D_0). Once determined, the thermal history is acquired by iterative fits to the age spectrum. The Ar closure temperature (T_c) for biotite is

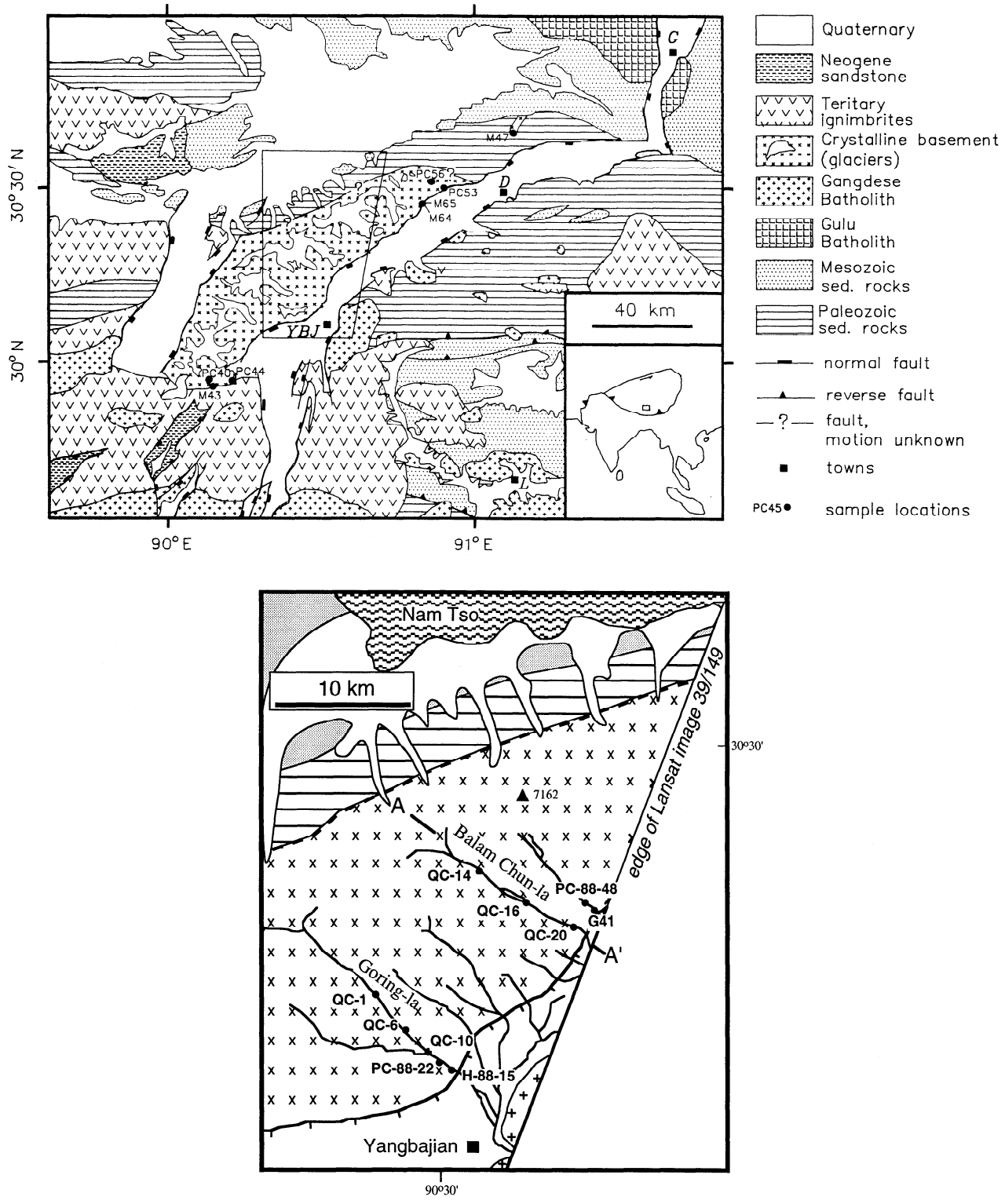

Figure 2. (a) Generalized geologic map of the Nyainqentanghla and surrounding region adapted from *Kidd et al.* [1988]. Abbreviations are D, Damxung; G, Gulu; L, Lhasa; YBJ, Yangbajian. The region encompassed by the polygon is shown expanded in Figure 2b. The inset shows the location of the geological map on a sketch map of Asia. (b) Sample location map showing the positions of the Goring-la and Balum Chun valleys. The drainage immediately NE of the Balum Chun valley is the Parnulang valley.

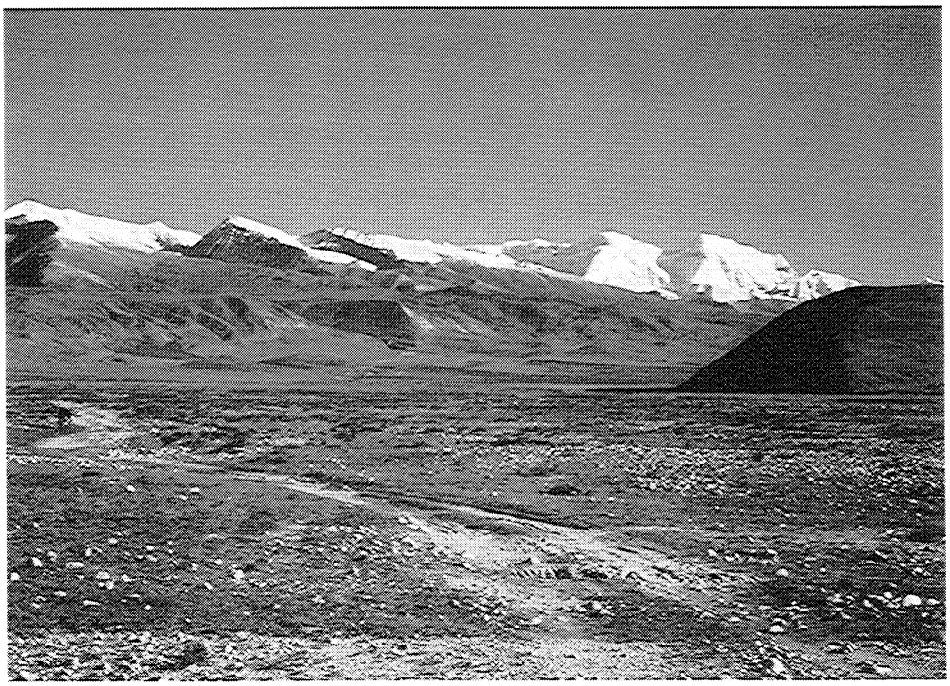

Figure 3. Photograph of the central part of the Nyainqentanghla from near Yangbajian showing the prominent dip slope (view to the north). The slope dips at ~25° to the SE and consists of mylonitic orthogneiss.

calculated assuming ρ = 330 μm, E = 47 kcal/mol, and D_o = 0.077 cm^2/sec [*Harrison et al.*, 1985; *Copeland et al.*, 1987]. The T_c of fission tracks in apatite is assumed to be 100±10°C [*Naeser*, 1981].

Northern Nyainqentanghla

Two distinct granite types were collected from the northernmost drainage in which igneous and metamorphic rocks are exposed (Figure 2a). PC-88-53 is from a small, unfoliated leucogranite (elevation 4880 m) with an intrusive contact against staurolite schist. PC-88-56 was collected ~3 km further up the valley (elevation 5020 m) and is a slightly more melanocratic granite whose margins are obscured by glacial deposits. Muscovites from these two samples yield essentially concordant $^{40}Ar/^{39}Ar$ ages of ~9 Ma.

K-feldspars from these two samples yield similar, but complex, $^{40}Ar/^{39}Ar$ age spectra (Figure 4). Their spectra are characterized by initially old ages that abruptly fall to a minima of ~6 Ma at about 40% ^{39}Ar released. Subsequent gas released yields apparent ages significantly older than the coexisting muscovites. The early gas release from PC-88-56 K-feldspar yields an isochron with a Mean Square of Weighted Deviates (MSWD) of 1.6, an age of 4.1±1.4 Ma, and $(^{40}Ar/^{36}Ar)_i$ = 1720±340. The higher temperature steps are suggestive of an age of ~17 Ma but this is probably not meaningful as the corresponding Arrhenius data indicate a maximum T_c of only about 320°C, less than that generally assumed for muscovite, which gives an age of 9 Ma. It seems likely that this apparent alignment of data results from non-atmospheric trapped argon. The age of ~4 Ma corresponds to a T_c of ~240°C.

Maximum ages from K-feldspar PC-88-53, the sample closer to the edge of the range and 140 m lower than PC-88-56, are in the range 12 to 14 Ma; the minimum age for this sample is 6 Ma. Defining the trapped argon composition of this sample is more difficult than for PC-88-56 as the data do not suggest a linear array on the isochron plot. Since the apatite fission track age for PC-88-56 is 5.1±0.6 Ma [*Pan et al.*, 1993], we can infer that the sample experienced rapid cooling from ~230°C (the approximate T_c of the small domains) at 6-5 Ma. Two float blocks of pelitic schist (M64-5 and M65-1) sampled from a drainage ~8 km to the SW (Figure 2a) both show concordant muscovite and biotite $^{40}Ar/^{39}Ar$ ages of ~8 Ma.

Approximately 40 km NE of samples PC-88-53 and 56, a ~1 km wide band of quartz-plagioclase-muscovite-biotite-garnet-staurolite schist is within a sequence of rocks unconformably overlain by a series of weakly metamorphosed sandstones, conglomerates, and (Cretaceous?) carbonates and exposed in apparent fault contact with a sequence of phyllites. *Harris et al.* [1988] interpreted the muscovite in this schist to be post tectonic and retrogressive; muscovite from M47-7, a sample of this schist (Figure 2a), gives an $^{40}Ar/^{39}Ar$ age of 155±2 Ma over 85% of the ^{39}Ar released. This age is similar to the timing of a fold and thrust belt 500 km to the west along strike, near Coquen (T.M. Harrison, unpublished data, 1993), and may reflect deformation associated with collision of the Lhasa block in Late Jurassic/Early Cretaceous time.

Central Nyainqentanghla

The eastern margin of the central Nyainqentanghla is bounded by a thick (~300 m), mylonitic high strain zone with a top-to-the SE shear sense [*Coward et al.*, 1988; *Pan and Kidd*, 1992]. The shear zone is characterized by prominent ~25°E dip slopes and hogbacks which extend to elevations greater than 6500 m (Figure 5). It is cut out to the NE and SW by younger

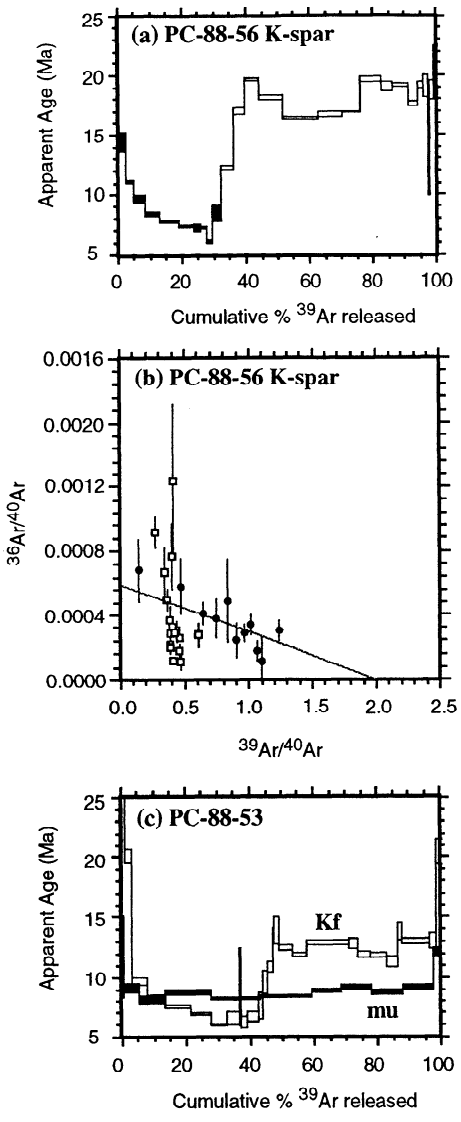

Figure 4. (a) $^{40}Ar/^{39}Ar$ age spectrum for K-feldspar PC-88-56, (b) isochron diagram for K-feldspar PC-88-56, and (c) age spectra for K-feldspar PC-88-53 K-feldspar and muscovite.

and steeper normal faults that bound the present graben [*Pan and Kidd*, 1992]. Ten samples were collected from within and beneath the shear zone and separated minerals analyzed by the $^{40}Ar/^{39}Ar$ method. Since the ductile quartz mylonitic structures formed at temperatures of at least 300°C [*Pan and Kidd*, 1992], thermochronological results that straddle this temperature should in principle permit us to constrain the timing of fault motion. Sample collection traverses were made through two valleys that cut the range: the Goring-la in the south and the Balum Chun to the north (Figure 2b). A short (1.5 km) traverse was also made into the Parnulang valley (Figure 2b) which runs parallel to, and about 2 km north of, the Balum Chun (Figure 2b). For purposes of discussion we have combined the results from the Balum Chun and Parnulang valleys.

Balum Chun Valley. Five samples of biotite granite and granitic gneiss from along the nearly horizontal (vertical separation ~350 m) traverses of the Balum Chun and Parnulang valleys have been analyzed by the $^{40}Ar/^{39}Ar$ method and the more recently produced K-feldspar results processed using the multidiffusion domain model. This analysis yields thermal history segments typically in the range 350° to 150°C. These results are supplemented by $^{40}Ar/^{39}Ar$ analyses of biotite and apatite fission track [*Pan et al.*, 1993] data. A schematic cross section of this traverse is shown in Figure 5.

Sample QC-14-92, a homogeneous medium-grained biotite granite, comes from the top of the Balum Chun traverse at an elevation of 5200 m. The K-feldspar yields an age spectrum characterized by initial ages of ~7 Ma that smoothly rise to ~12 Ma (Figure 6a). The Arrhenius plot yields an E = 48.8 kcal/mol and is well-modeled assuming nine diffusion domains that vary in size by 4 orders of magnitude (Figures 6b and 6c). These Arrhenius and domain distribution parameters yield a good fit to the age spectrum assuming the thermal history shown in Figure 6d. We estimate uncertainties in the K-feldspar-derived thermal histories, shown by the bold segment, to be ±25°C and ±0.2 Ma. From an initial temperature of 340°C at 12 Ma, cooling proceeds at 5°C/m.y. until 7.1 Ma when temperature drops rapidly (~150°C/m.y.). The coexisting biotite age of 9.0±0.2 Ma and assumed T_c agree within uncertainty with this thermal history.

QC-16-92, a weakly-foliated biotite granite, was sampled 4 km to the SE of QC-14-92 (elevation 5170 m). Initial ages in the spectrum (Figure 7a) show the saw-toothed pattern characteristic of Cl-correlated excess ^{40}Ar released from decrepitating fluid inclusions [*Harrison et al.*, 1993a, 1994]. The isothermal duplicate steps used in the heating schedule of this and most other analyses permit us to see through this contamination, as the second step at a given temperature is largely free of the excess ^{40}Ar. Corrected ages rise from 5.3 Ma to ~10 Ma. Using our automated routine to assess E, a value of 38.4 kcal/mol was identified for this K-feldspar. This value is anomalously low relative to the other seven samples (E = 46±2 kcal/mol) and yields a thermal history that is not in agreement with the coexisting biotite datum (7.5±0.1 Ma). Thus for this thermal calculation, we have assumed E to be the average value of the other K-feldspars from the Nyainqentanghla (46 kcal/mol). This results in a reasonable fit to the Arrhenius data (Figures 7c and 7d) and yields a thermal history in closer agreement with the biotite result. This result is a reminder that low apparent E values can result from mixing between small domains of low volume fraction [e.g., *Heizler and Harrison*, 1991]. The age spectrum and calculated thermal history indicate that rapid cooling at this location began at 5.2 Ma.

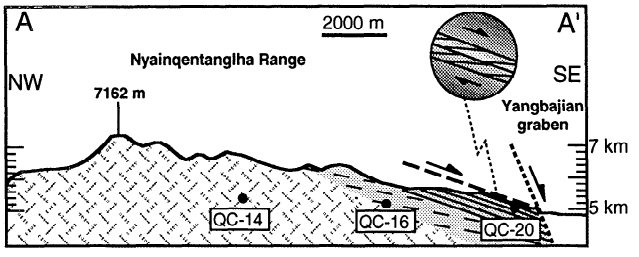

Figure 5. Schematic NW-SE cross section through the Nyainqentanghla showing the approximate orientation of the shear zone, active normal fault, and the relative locations of three Balum Chun samples (Adapted from *Pan and Kidd* [1992]).

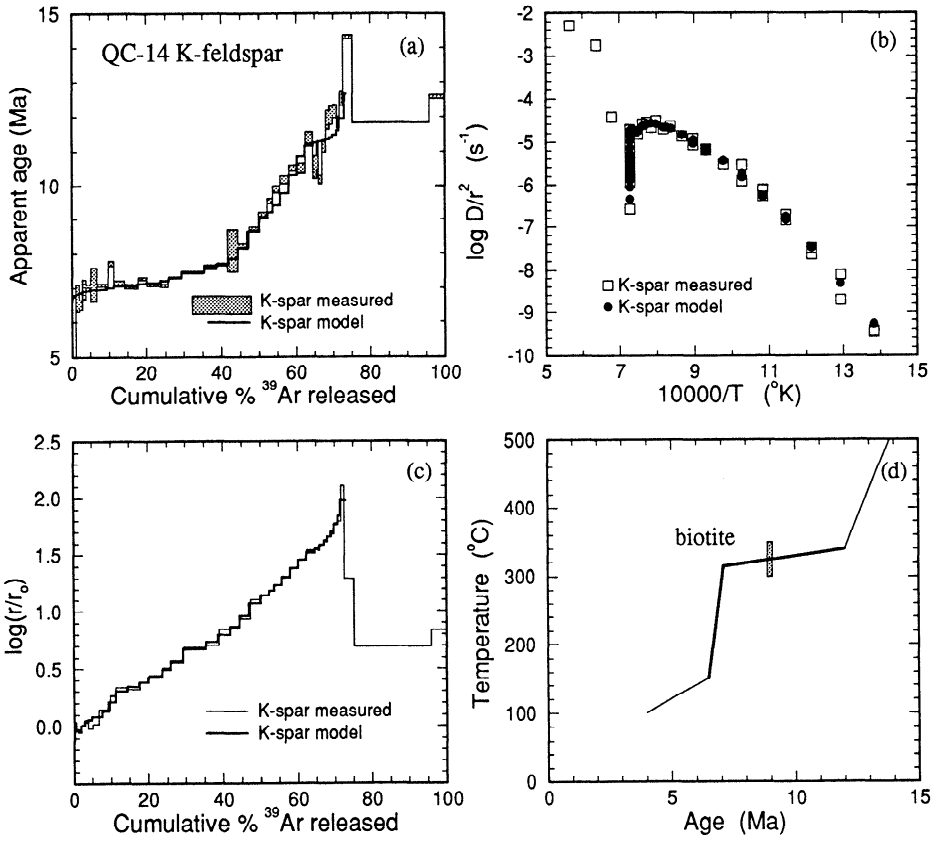

Figure 6. The $^{40}Ar/^{39}Ar$ results for K-feldspar QC-14-92, Balum Chun valley: (a) age spectrum, (b) Arrhenius plot, (c) log (r/r_o) plot, and (d) thermal history (also showing biotite T-t datum).

QC-20-92 is a mylonitic orthogneiss from within the detachment fault shear zone about 1 km from the bottom of the Balum Chun valley (elevation 4840 m). S-C fabrics are well-developed along with a strong lineation (308°/10°SE). Some chloritic surfaces are present. The $^{40}Ar/^{39}Ar$ age spectrum of the K-feldspar, again showing the saw-toothed excess ^{40}Ar pattern, rises from ages of 3 to 4 Ma in a smooth fashion to a plateau at 9 Ma (Figure 8a). The Arrhenius and distribution parameters were selected by an automated routine and produce an excellent fit to the log (r/r_o) plot (Figure 8c). The thermal history is characterized by rapid cooling that began at 3.5 Ma (Figure 8d).

Samples from two locations along the Parnulang valley were also analyzed for this study. Because of their close proximity to the Balum Chun, we have included these results in the subsequent modeling and discussion of the Balum Chun. Sample PC-88-48 is from a nearly identical structural position to QC-20-92, about 1.5 km from the SE margin of the high strain zone (elevation 4960 m). Steps 3-18 show a saddle like shape on the age spectrum (Figure 9a) but define a linear array (MSWD = 4) on an isochron diagram with an age of 3.7±0.1 Ma and an $(^{40}Ar/^{36}Ar)_i$ of 760±40. The final portion of gas released from K-feldspar PC-88-48 (steps 21-32) yields a flat segment on the age spectrum at ~8 Ma as well as a line (MSWD = 0.6) on the isochron diagram with an age of 8.1±0.1 Ma and $(^{40}Ar/^{36}Ar)_i$ = 275±29. Similar plots for the high-temperature plateau like segments for QC-14-92, QC-16-92, and QC-20-92 also show linear arrays with atmospheric intercepts. This sample was analyzed before our current laboratory protocols were in place, and thus the Arrhenius results are not as well controlled as those for the more recently measured samples. Nonetheless, an E = 46.4 kcal/mol and four diffusion domains differing in size by ~2.5 orders of magnitude yield a reasonably good fit to the Arrhenius plot (Figures 9b and 9c). As with QC-20-92, the thermal history indicates rapid cooling beginning at ~4 Ma. Biotite from PC-88-48 yields a plateau over 82% of the ^{39}Ar released with an age of 6.2±0.1 Ma.

K-feldspar from sample G41, collected at the bottom of the Parnulang valley immediately below the ultramylonites which mark the top of the shear zone (elevation 4800 m), yields a complex age spectrum with two apparent ages of 4.1 and 7.8 Ma. Only approximate temperature limits can be placed on these segments as over 50% of the ^{39}Ar was released at temperatures above K-feldspar melting: ~200°C for the younger age and a lower limit of 225°C for the upper plateau. The age of the younger plateau is similar to that of PC-88-48 and the apatite fission track age from adjacent to sample P-72-1 of 3.3±0.6 Ma [*Pan et al.*, 1993]. Together, these results from the bottom of the Parnulang valley indicate very rapid cooling (>100°C/m.y.) from ~230 to 100°C at 4-3 Ma.

Goring-la Valley. The Goring-la is a deeply incised valley parallel to and about 15 km to the SW of the Balum Chun that leads to the only pass across the range. QC-1-92 is a pelitic gneiss within a migmatitic injection zone sampled at the NW end of this traverse (elevation 5000 m). The K-feldspar

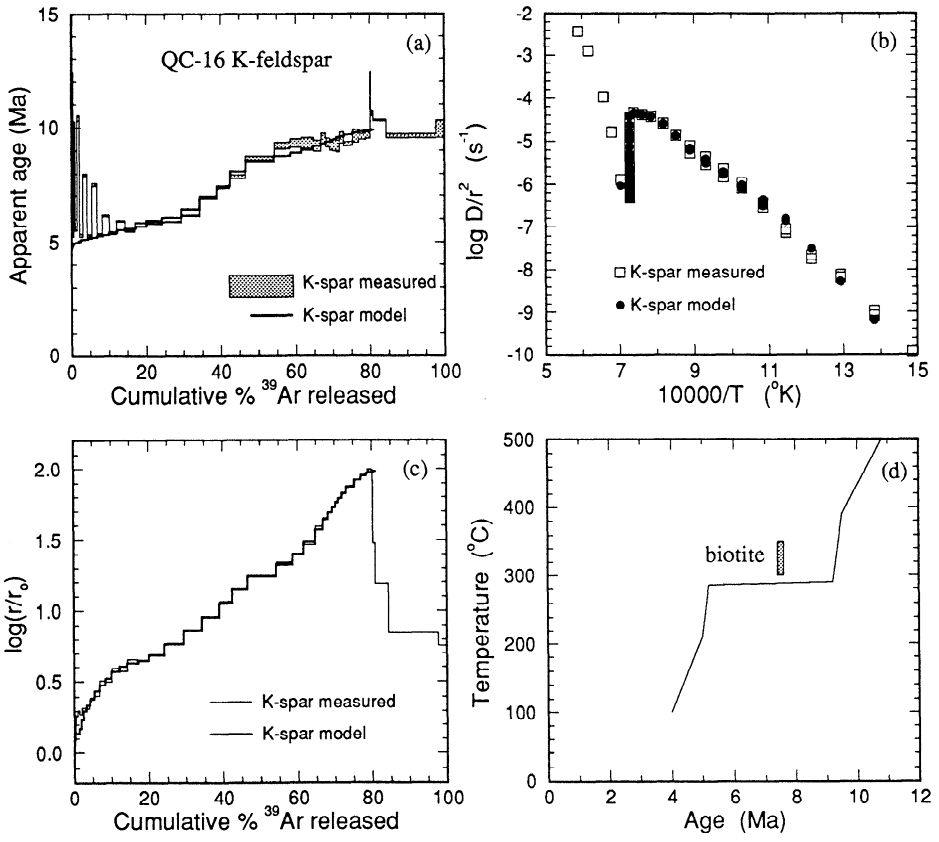

Figure 7. The $^{40}Ar/^{39}Ar$ results for K-feldspar QC-16-92, Balum Chun valley: (a) age spectrum, (b) Arrhenius plot, (c) log (r/r_o) plot, and (d) thermal history (also showing biotite T-t datum).

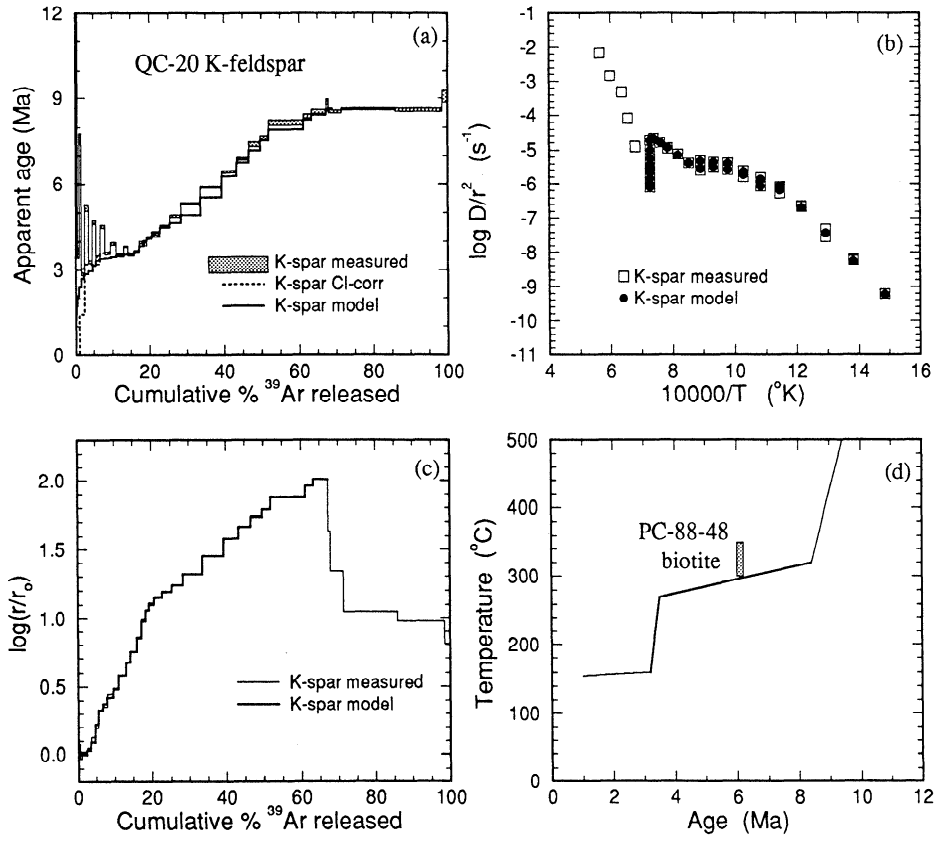

Figure 8. The $^{40}Ar/^{39}Ar$ results for K-feldspar QC-20-92, Balum Chun valley: (a) age spectrum, (b) Arrheniu plot, (c) log (r/r_o) plot, and (d) thermal history (also showing biotite T-t datum).

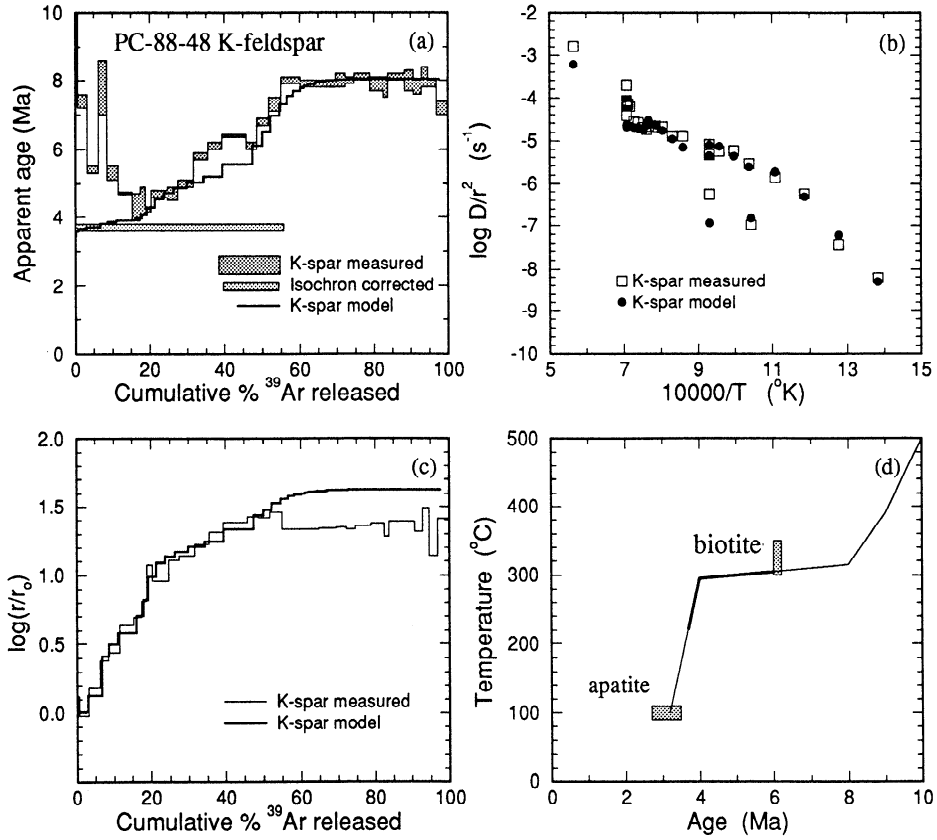

Figure 9. The $^{40}Ar/^{39}Ar$ results for K-feldspar PC-88-48, Parnulang valley: (a) age spectrum, (b) Arrhenius plot, (c) log (r/r_o) plot, and (d) thermal history (also showing apatite and biotite T-t data).

$^{40}Ar/^{39}Ar$ age spectrum (Figure 10a) yields initial ages of 5 to 6 Ma which climb smoothly to an age of 15.5±0.3 Ma (isochron age for the last seven steps). The principal features of the calculated thermal history are the relatively slow cooling between 15 and 7 Ma, followed by rapid cooling at a rate of ~100°C/m.y. (Figure 10d). The coexisting biotite yields an age of 7.56±0.08 Ma which agrees with the K-feldspar-derived thermal history (Figure 10d).

About 3.5 km further to the SE of QC-1-92, sample QC-6-92 was obtained from a foliated biotite granite immediately above the injection zone. The K-feldspar $^{40}Ar/^{39}Ar$ age spectrum (Figure 11a) rises from ages of 4.5 to 5.0 Ma to an age of 9.4±0.1 Ma. The calculated thermal history indicates that the sample cooled at a rate of ~20°C/m.y. from 9-5 Ma, followed by rapid cooling (>80°C/m.y.) (Figure 11d). The coexisting biotite yields an age of 6.59±0.07 Ma which is consistent with the K-feldspar-derived thermal history.

QC-10-92 (elevation 4630 m) comes from a moderate S-C granite mylonite 2.5 km from the bottom of the Goring-la. The K-feldspar $^{40}Ar/^{39}Ar$ age spectrum (Figure 12a) shows a pronounced saw-toothed pattern over the first ~20% of gas release but suggests an age of about 4 Ma. Correction for the Cl-correlated excess ^{40}Ar yields ages between ~3 and 4 Ma for this portion of release. Ages then rise to ~11 Ma. The coexisting biotite yields an age of 5.4±0.1 Ma.

About 400 m from the bottom of the valley, a ~5-m sized block of amphibolite and calc-silicate gneiss sits discordantly within the granite gneiss. The foliation in this block, which trends NW and has a vertical dip, is orthogonal to the foliation of the host mylonite. It is not clear whether this block was incorporated into the granitic material that surrounds it during a magmatic stage or during the deformation which produced the fabric in the granitic gneiss. A ~10-cm-wide, completely recrystallized leucocratic vein composed of quartz, K-feldspar, sphene and pyroxene (ferrosalite), cuts the main foliation of the calc-silicate gneiss (Figure 13) but does not penetrate into the sheared rocks; neither were dikes of similar composition found nearby. The vein appears to have intruded into this block prior to its incorporation into the granite gneiss and thus predates the shearing deformation in the granite gneiss. K-feldspar from a sample of the dike (H-88-15; elevation 4500 m) yields two linear arrays on a $^{40}Ar/^{39}Ar$ isochron (Figure 14a): steps 5-18 give a flat segment on the age spectrum and an array on the isochron diagram corresponding to an age of 4.3±0.2 Ma and a $(^{40}Ar/^{36}Ar)_i$ of 291±7 (MSWD = 1.1), whereas steps 25-36 yield a relatively well-fitting line (MSWD = 4.0) with an age of 5.6±0.2 Ma and a $(^{40}Ar/^{36}Ar)_i$ of 310±6. The Arrhenius data for this K-feldspar (Figure 14b) indicate an E = 44 kcal/mol and six domains that vary in size by about 2 orders of magnitude, but again these results were obtained prior to optimization of the laboratory heating schedule. They constrain a slow cooling portion of the thermal history (Figure 14d) from 5.6 Ma at 305°C to 4.4 Ma at 295°C at which point rapid cooling began with the temperature dropping below 100°C by 3.6±0.5 Ma, as

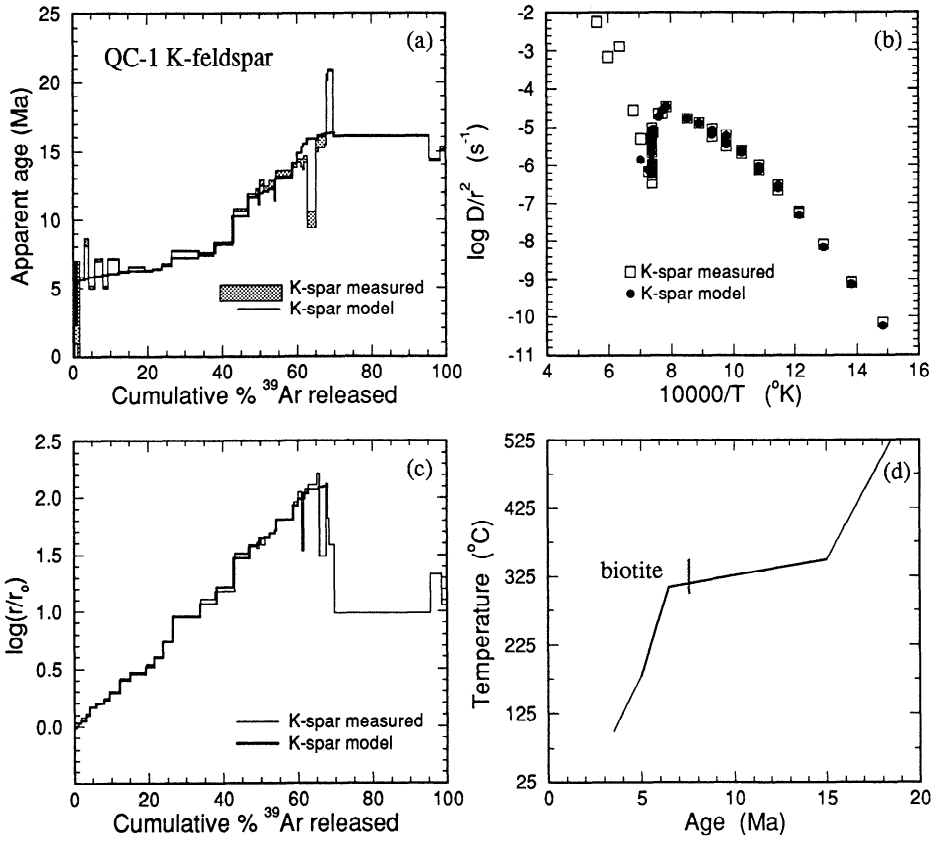

Figure 10. The $^{40}Ar/^{39}Ar$ results for K-feldspar QC-1-92, Goring-la valley: (a) age spectrum, (b) Arrhenius plot, (c) log (r/r_o) plot, and (d) thermal history (also showing biotite T-t datum).

evidenced by the apatite fission track date [*Pan et al.*, 1993] from a sample (P-28-1) obtained 500 m upstream from H-88-15.

Sphene in sample H-88-15 is subhedral to euhedral and up to 3 mm long. Duplicate analyses yield a $^{206}Pb/^{238}U$ sphene/K-feldspar model age of 11.2±0.3 Ma (Kevin Chamberlin, personal communication, 1989). Using the diffusion parameters of *Cherniak* [1993], the T_c for Pb in sphene (ρ = 0.15 cm, dT/dt = 10°C/m.y.) is estimated to be ~620°C. This value is in general agreement with empirical estimates [*Metzger et al.*, 1991]. Because of the small proportion of radiogenic Pb in the sphene (~12%), however, it is possible that Pb exchange during low-temperature alteration or deformation of the feldspar could result in an underestimate of the sphene closure age.

A sample of amphibolite (PC-88-22) was collected from the same outcrop, about 3 m from H-88-15. Hornblende from this rock yields a complex age spectrum with apparent ages ranging between ~22 and 11 Ma (Figure 15). This complex behavior can be understood with reference to the isochron (steps 3-11, or ~70% of the ^{39}Ar released) which corresponds to an age of 6.5±0.9 Ma and a $(^{40}Ar/^{36}Ar)_i$ of 626±30 (Figure 15). The question arises as to whether this age reflects closure with respect to diffusion at high temperature (~450-500°C) [*Baldwin et al.*, 1990] or continued recrystallization to much lower temperatures (say, 350°C). We do not have sufficient information to completely resolve this question, but it seems unlikely that volume diffusion would have been the rate limiting step in argon loss from the hornblende during continued deformation. The question of closure versus recrystallization needs also be addressed to the K-feldspar results from within the shear zone, for although their highest temperatures of argon retention are only slightly above those estimated for the brittle-ductile transition (~350°C [*Carter and Tsenn*, 1987]), recrystallization could have reset the domain structure subsequent to closure. Our principal argument to the contrary is the broadly systematic nature of the results obtained from both below and within the shear zone (Figure 16).

Thermal history results from the Balum Chun (Figures 6d-9d) and Goring-la (Figures 10d-12d and 14d) traverses show systematic variations that permit some insight into the thermomechanical evolution of the detachment system. Biotites show a trend of decreasing ages from top to bottom of the Goring-la of 7.56±0.08, 6.59±0.07, and 5.4±0.1 Ma (samples QC-1-92, QC-6-92, and QC-10-92, respectively), and from top to bottom of the Balum Chun (and Parnulang) of 9.0±0.2, 7.5±0.1, and 6.2±0.1 Ma (QC-14-92, QC-16-92, PC-88-48, respectively). With the exception of sample QC-10-92, the K-feldspar data reveal the progression of a rapid cooling event from ~8-7 Ma in the core of the range to ~4-3 Ma within the shear zone (Figure 16). The thermal history calculated for QC-10-92 K-feldspar is discordant to the others in the Goring-la in that it predicts relatively low temperatures (~300-350°C) within the shear zone between 11 and 6 Ma. However, the thermal history for QC-10-92 would come into agreement with the overall cooling pattern if ages older than ~8 Ma were due to the

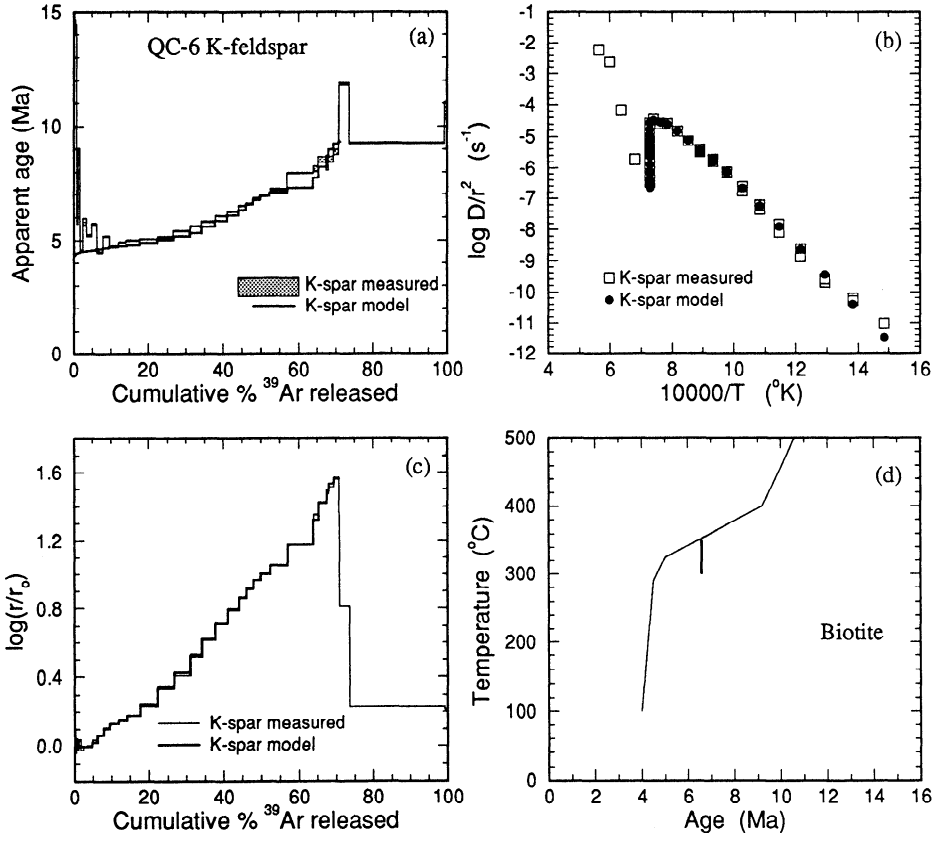

Figure 11. The $^{40}Ar/^{39}Ar$ results for K-feldspar QC-6-92, Goring-la valley: (a) age spectrum, (b) Arrhenius plot, (c) log (r/r_o) plot, and (d) thermal history (also showing biotite T-t datum).

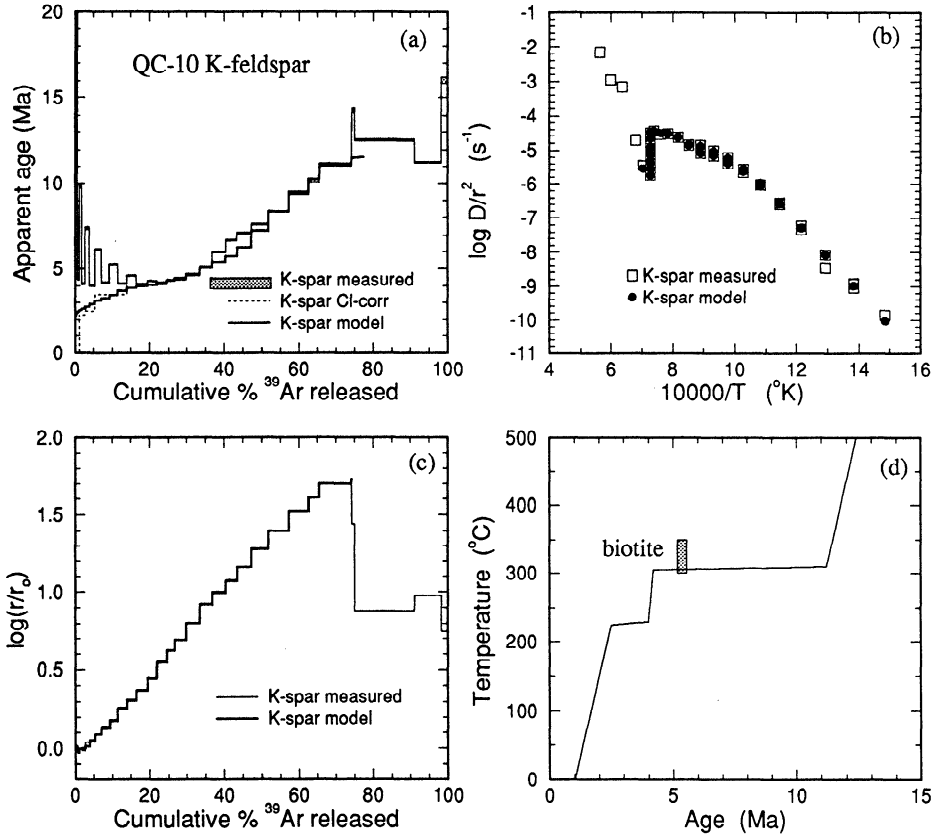

Figure 12. The $^{40}Ar/^{39}Ar$ results for K-feldspar QC-10-92, Goring-la valley: (a) age spectrum, (b) Arrhenius plot, (c) log (r/r_o) plot, and (d) thermal history (also showing biotite T-t datum).

Figure 13. Photograph of a leucocratic dike and calc-silicate gneiss in the Goring-la Valley of the Nyainqentanghla. The dike has a foliation which is weaker but similar in orientation to the host block, which is itself discordant to the fabric in the country rock.

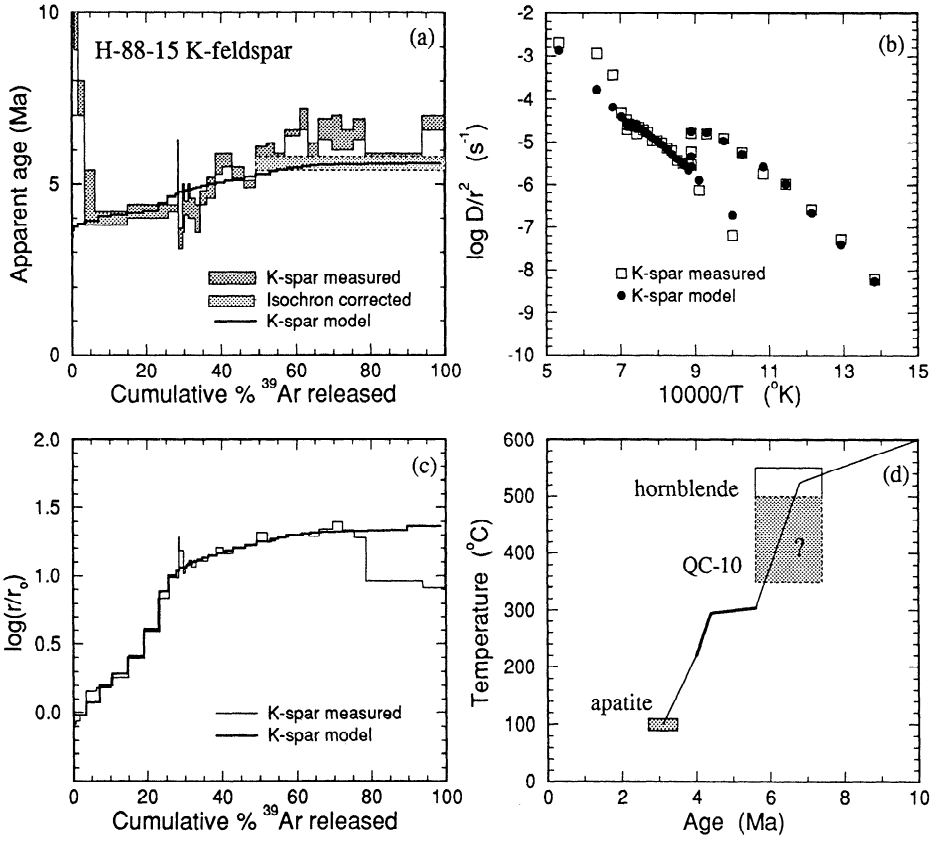

Figure 14. The $^{40}Ar/^{39}Ar$ results for K-feldspar H-88-15, Goring-la valley: (a) age spectrum, (b) Arrhenius plot, (c) log (r/r_o) plot, and (d) thermal history (also showing apatite and hornblende T-t data). Results from heating steps 5-18 define an isochron with an age of 4.3±0.2 Ma and a $(^{40}Ar/^{36}Ar)_i$ of 291±7. Steps 25-36 define a second line with an age of 5.6±0.2 Ma and a $(^{40}Ar/^{36}Ar)_i$ of 310±6.

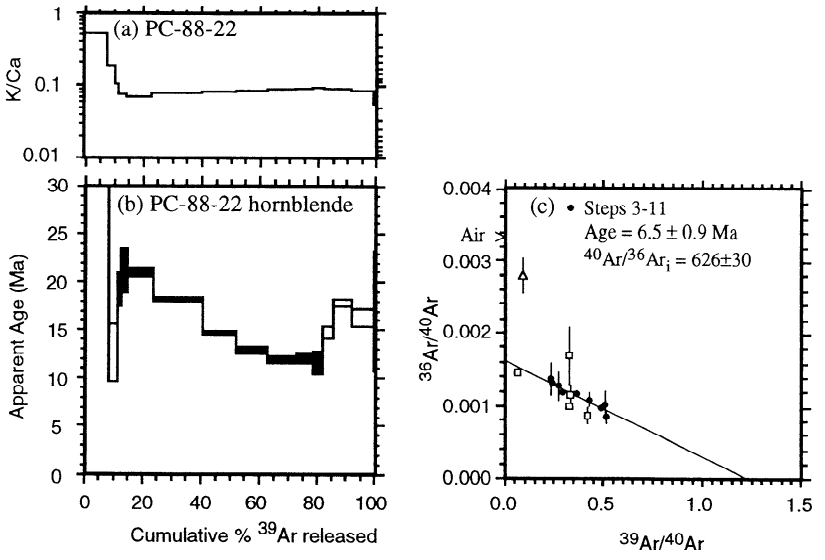

Figure 15. (a) K/Ca, (b) age spectrum, and (c) isochron plots for hornblende PC-88-22, Goring-la valley. Steps 3-11 (solid circles) define an isochron age of 6.5±0.9 Ma and $(^{40}Ar/^{36}Ar)_i$ of 626±30. The first two steps show a high K/Ca ratio suggestive of biotite contamination.

presence of excess argon. It is not possible to confirm this speculation one way or the other, however, as the high temperature data do not define an isochron. However, because of this possibility, and the fact that the thermal history predicted for QC-10-92 is contradicted by results from nearby samples H-88-15 and PC-88-22, we have chosen to not consider data obtained from this sample in our overall interpretation.

Southern Nyainqentanghla

The southern part of the range, near Shigula (Tenfen) Pass, is dominated by peraluminous granites (±garnet-bearing). One of these granites, PC-88-40 (elevation 5510 m) yields a biotite $^{40}Ar/^{39}Ar$ age of 10.1±0.1 Ma and a K-feldspar age spectrum with two apparent ages at ~9.5 Ma and 12.5 Ma. The Arrhenius results for this sample suggest that this age range corresponds to temperatures between 230 and 330°C. Sample K-88-56, collected nearby at the top of the pass (elevation 5520), yields an apatite fission track age of 5.3±0.6 Ma [*Pan et al.*, 1993] indicating continued cooling at ~30°C/m.y. in the interval 9-5 Ma. M43-1, a float block of two-mica granite collected along the road below PC-88-40, yields muscovite and biotite $^{40}Ar/^{39}Ar$ isochron ages of 14.6±0.1 and 13.0±0.1 Ma, respectively. K-feldspar from this sample has an age gradient ranging from 9.5 to 15 Ma with a T_c of the small diffusion domains estimated from the Arrhenius data to be ~275°C. Because over 50% of the ^{39}Ar was released from this sample above the onset of melting, we can only estimate a minimum T_c of the largest diffusion domain of ~330°C. The oldest age from the K-feldspar is equal to the muscovite age of ~15 Ma, suggesting the maximum T_c in the K-feldspar of ~350°C. Along the eastern margin of the range, a small outcrop of amphibolite is exposed next to the road. Hornblende from this outcrop (PC-88-44) yields a spectrum with an age of ~100 Ma. The young ages in the first three steps of this age spectrum have high K/Ca ratios and likely reflect minor biotite contamination.

Discussion

Thermal and Mechanical Evolution of the Nyainqentanghla Shear Zone

Numerical model. We presume that the two styles of extensional faulting observed on the east side of the Nyainqentanghla (i.e., the earlier mylonitic shear zone and active high angle faults) are consecutive manifestations of the same evolving system. Because closure temperatures are generally >200°C, our thermal history results record tectonic information related only to the earlier phase of normal faulting. However, average slip rates for the subsequent phase of normal faulting have been constrained, albeit with lesser precision, using geomorphological methods [*Armijo et al.*, 1986].

Thermal history results from both valleys in the central Nyainqentanghla indicate a progression of rapid cooling from ~8 Ma in the core of the range to ~4 Ma within the shear zone. We proceed with analysis of these results on the assumption that movement on the detachment fault at middle crustal depths initiated at an angle closer to 60° than the presently observed dip of 25° [e.g., *Jackson and McKenzie*, 1983] but will return to this question later. The high angle geometry implies that the samples from the top and bottom of each valley, presently subhorizontal, were once vertically separated by about 5 km. To extract tectonic information from the cooling histories, we have modeled their thermal evolution following slip on a normal fault using a finite-difference solution to the generalized equation and boundary condition:

$$\frac{\partial T}{\partial t} = \kappa \nabla^2 T - \mathbf{V} \cdot \nabla T + \frac{A_o}{\rho c} \qquad (1)$$

$$\mathbf{n} \cdot \nabla T = -\sigma V \quad \text{on the fault surface}$$

where T is temperature, t is time, κ is thermal diffusivity, V is slip velocity, A_o is heat generation, ρ is density, c is heat

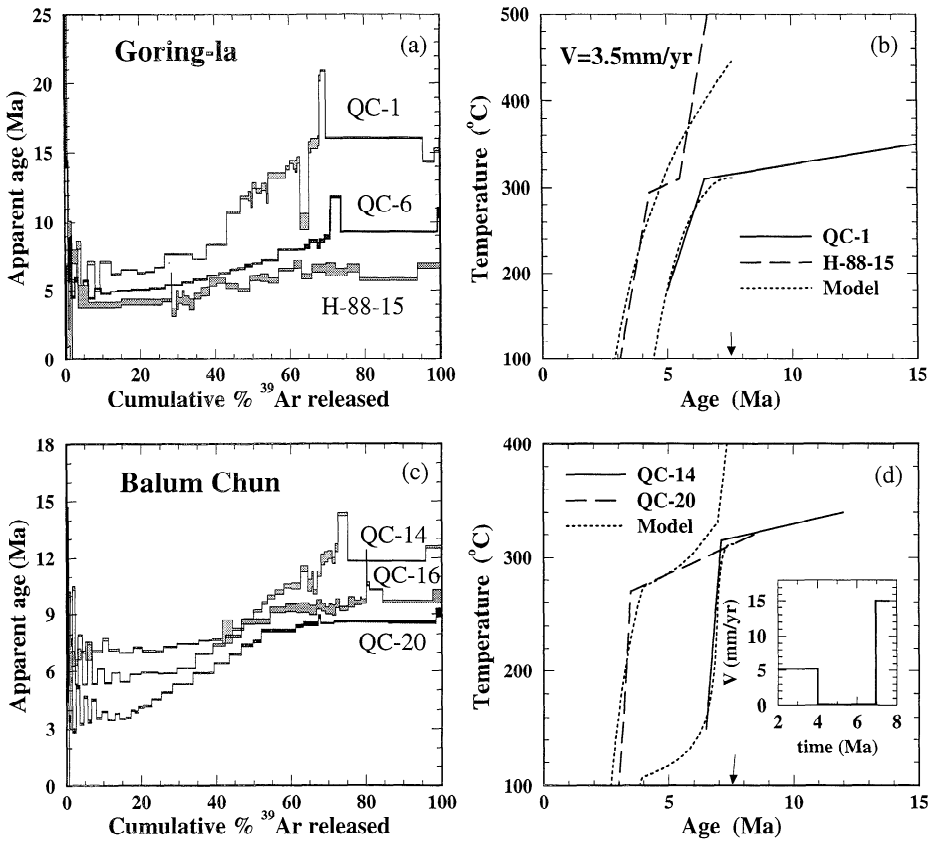

Figure 16. (a) Goring-la age spectra and (b) isotopically derived thermal histories shown together with results from forward modeling to the thermal histories from the locations at the top and bottom of the valley. The model fit (dashed lines) assumes faulting began at 7.6 Ma (shown by the arrow) at a rate of 3.5 mm/yr. (c) Balum Chun age spectra and (d) isotopically derived thermal histories together with forward modeling results (dashed lines) for the top and bottom of the valley. The model fit is based on fault initiation at 7.6 Ma (shown by the arrow) with the slip history shown in the inset in Figure 16d.

capacity, σ is flow stress, and **n** is the normal to the fault surface. However, reasonable estimates of the frictional (σV) heating parameter suggest it to be a negligible contribution to the total heat budget. We have fixed most parameters in the numerical simulations using average values for midcrustal rocks (i.e., $\kappa = 10^{-6}$ m^2/sec, $A_o = 10^{-6}$ W/m^3, $\rho = 2850$ kg/m^3, $c = 1000$ J/kg-°C, and $\sigma = 50$ MPa) as expected variations from these values are unlikely to affect the outcome of the calculations at the level of confidence we accept for timing of fault initiation (i.e., ±1 Ma) and average slip rate (±50%).

The numerical scheme utilizes an explicit method to obtain the temperature offset resulting from an increment of movement on the fault that is then relaxed using the alternating direction implicit method [e.g., *Peaceman and Rachford*, 1955]. The boundary conditions are fixed such that slip on the fault produces uplift of the footwall block that is maintained at a constant surface elevation by erosion. This scheme is similar to that used by *Ruppel et al.* [1988] to model thermal histories arising from a simple shear geometry. Incorporating both realistic erosion conditions (i.e., surface topography, variable erosion rates) and syntectonic changes in fault geometry (i.e., domal exposure, rotation of the fault surface) into the model is expected to have either compensatory influences on the predicted cooling histories or markedly change them only when the sample is relatively close to the surface.

The distribution of isotherms prior to initiation of normal faulting and that following 5 m.y. of slip at 3.5 mm/yr are shown together in Figure 17. Also indicated are the positions we interpret to be the top (circles) and bottom (squares) of the two central Nyainqentanghla traverses. The temperature histories predicted for locations corresponding to the top and bottom of the valleys vary considerably with assumed slip rate. In general, the structurally higher valley tops cool mainly due to surface erosion, whereas the rocks in the shear zone cool due to both erosional and tectonic denudation. For slip rates on the order of a few millimeters per year (see Figure 17), the initial temperature difference between the two vertically separated positions tends to be maintained. In contrast, relatively rapid slip rates (>10 mm/yr) result in the two vertically separated positions achieving a similar temperature before the structurally higher region begins to cool rapidly due to the approaching surface.

Age of detachment faulting and slip history. The ^{40}Ar/^{39}Ar data from the southern part of the range suggest that cooling through the temperature range 350 to 230°C occurred between 15 and 9 Ma with continued rapid cooling subsequently. The northern portion of the range cooled through this temperature

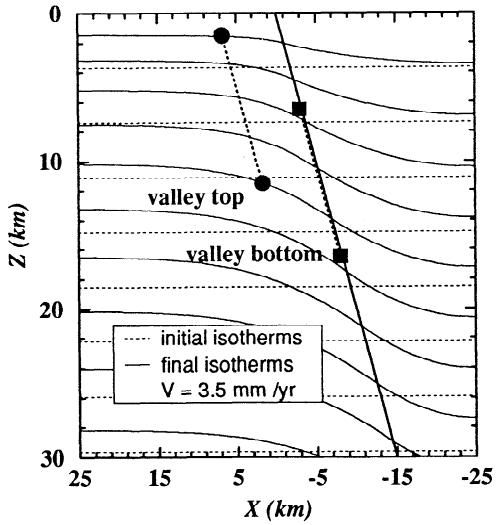

Figure 17. Distribution of isotherms prior to initiation of normal faulting (dashed lines) and following 5 m.y. of slip at 3.5 mm/yr (solid lines). Locations appropriate to the top (QC-1-92) and bottom (H-88-15) of the Goring-la for these two times are shown by the circles and squares, respectively. The model assumes that slip on the fault produces uplift of the footwall that is maintained at constant surface elevation by erosion. The initial thermal gradient is 27°C/km.

range at about the same rate with rapid cooling beginning at ~8 Ma. Muscovite and biotite ages between 8 and 9 Ma from two float blocks of muscovite-biotite schist (M64-5, M65-1) and two granites separated by 140 m in elevation (PC-88-53, PC-88-56) are consistent with this history.

Age spectra and calculated cooling histories for the Goring-la samples (QC-1-92, QC-6-92, H-88-15) are shown together in Figures 16a and 16b. As remarked above, the form of the isotopically derived thermal histories is generally similar to the synthetic histories predicted by the model. We have placed the greatest weighted on the results from the top and bottom of each valley. Since these locations experienced the strongest thermal contrast within the traverse, they should provide us with the greatest control in selection of model parameters. We iteratively adjusted both slip rate and the timing of initiation of slip until a good fit to the empirical results was attained. In general, the thermal history from the top of the valley is the principal control on the timing of fault initiation, whereas the data from the bottom of the valley are the dominant constraint on the estimate of slip rate. For the Goring-la data, the best fit forward model was obtained using a relatively simple history; fault motion begins at 7.6 Ma with a constant slip rate of 3.5 mm/yr for a duration of 5 m.y. (Figure 16b). We find that varying the time of initiation from the preferred value by 1/3 m.y. leads to a mismatch with the empirical cooling history that exceeds our estimate of its accuracy and thus conservatively estimate the onset of detachment faulting at 8±1 Ma.

Age spectra and cooling histories for the Balum Chun samples (QC-14-92, QC-16-92, QC-20-92) are shown together in Figures 16c and 16d. Although a reasonably good model fit was obtained for these results, a more complex slip history is required to attain a similar degree of fit as that for the Goring-la data. Best fit was obtained using a model (Figure 16d) in which fault motion is assumed to begin at 7.6 Ma at a rate of 15 mm/yr for 0.6 m.y., drops to 0.1 mm/yr until 4 Ma, and then rises to 5 mm/yr (inset to Figure 16d).

The average slip rate of ~3.3 mm/yr estimated for the Balum Chun over the interval 7.6-2.6 Ma is similar to the model result from the Goring-la data of 3.5 mm/yr for the same period. Both are consistent with the range of Pleistocene slip rates (0.5-6 mm/yr) estimated for the Yangbajian graben by *Armijo et al.* [1986], and it is thus possible that normal faulting on the eastern edge of the Nyainqentanghla has proceeded at an essentially constant rate since initiation in the late Miocene. Although we emphasize that the results of the modeling are not unique, we are encouraged by the generally good model fits, the similarity of the average slip rates for the two valleys (~3 mm/yr) and congruity with estimates of slip rate subsequent to the main phase of detachment faulting [i.e., *Armijo et al.*, 1986], and the agreement between the two independent estimates of the timing of fault initiation (i.e., 7.6 Ma).

Isostatic adjustment following normal faulting elevates the footwall by about one-tenth the subsidence of the hanging wall [*Jackson and McKenzie*, 1983]. Whether or not coupled with flexural effects, this mechanism leads to differential unroofing of the footwall [e.g., *Buck*, 1988; *Weissel and Karner*, 1989]. The net result is that the section eventually exposed at the surface is an oblique slice through the footwall with the deepest exposures directly adjacent to the active normal fault [e.g., *Harrison et al.*, 1992a]. When the normal fault has rotated to a sufficiently low angle precluding further slip, a new fault may break at the higher optimum angle [e.g., *Proffett*, 1977]. We infer that this sequence of events is responsible for the present geometry of the Nyainqentanghla shear zone relative to the currently active normal faulting.

Assumption of high-angle normal faulting. Because the hanging wall strata of this ductile shear zone have been buried by Quaternary sedimentary rocks (Figure 2a), the original dip angle of the shear zone cannot be directly constrained by field relationships. An attempt to determine the dip angle of the detachment fault was made by exploiting shear zone rock paleomagnetism. Magnetic inclination and declination measurements were made on seven cores drilled from oriented samples obtained from across the Balum Chun transect (P. Copeland and S. Hall, unpublished data, 1993). Because the strike of the shear zone contains an E-W component, rotation of an originally high angle fault surface to a lower angle would lead to an apparent increase in the measured inclination permitting an estimate of the amount of rotation. However, the results that were obtained are complex and not easily interpreted (Figure 18). Although four of the seven samples yield inclinations of ~25°, expected for southern Tibet during the late Miocene, two measurements yield negative values and a third sample has an inclination of ~60°. Five of the seven declinations are in the range -20 to +60°, but the two samples from the middle of the transect yield values of about -150° suggesting that acquisition of magnetization within that portion of the transect may have occurred during a polarity reversal. Although these measurements surely contain important and interesting information, their bearing on the question at hand is not obvious and requires further study.

An alternate approach to test our assumption regarding slip

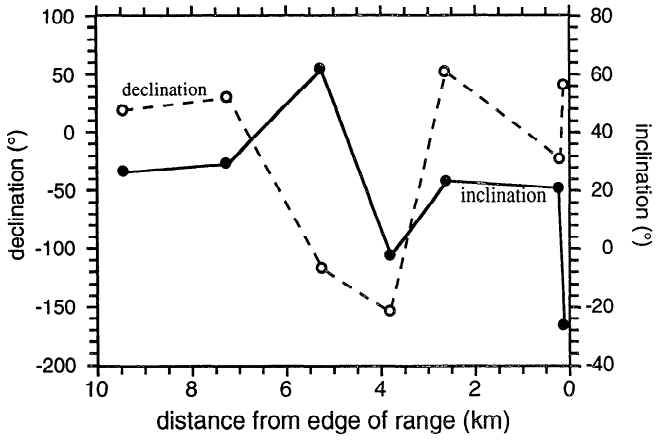

Figure 18. Magnetic inclination (solid circles) and declination (open circles) data for seven samples plotted as a function of their distance from the range front fault along the Balum Chun traverse.

angle is to use the thermal model to assess whether or not it is possible to achieve the form of the calculated temperature histories if the fault moved at a relatively low angle. Results of two simulations using slip angles of 63° and 27° are shown in Figure 19. When slip occurs at high angle (i.e., 63°), the sample at the top of the valley remains cooler than the sample adjacent to the normal fault at all times, in accord with our observations, regardless of whether the slip rate is 3.5 or 20 mm/yr (Figure 19b). Note that because we have not allowed footwall surface topography, our model results are constrained to yield rapid cooling earlier than if surface uplift was permitted. This would in part be mitigated by rotation of the footwall, and on balance we conclude that this effect would not significantly alter the predicted thermal histories. In contrast, slip occurring close to the presently measured angle (27°), whether rapid or slow, results in nearly identical cooling histories from both ends of the valley (Figure 19a), with periods during which the sample location at the top is hotter than the base of the valley (i.e., the opposite of what we observe). Because our thermal history results indicate that cooling to a given temperature was first achieved by samples at the top of the valleys and proceeded toward the bottom, we conclude that there must have been significant structural relief separating the ends of our valley transects and therefore that slip must have been initiated at relatively high angle (>40°).

Implications for Tectonics and Climate

Prior estimates place graben initiation in both the Himalaya [*Mercier et al.*, 1987; *Coleman and Hodges*, 1995] and on the Tibetan plateau [*Armijo et al.*, 1986; *Harrison et al.*, 1992b] during the late Neogene. The inferred presence of Pliocene and late Miocene beds in the Himalayan Thakkhola graben (Figure 1) suggested to *Mercier et al.* [1987] that the change from a contractional to an extensional regime probably occurred there during late Miocene time (i.e., between 11 and 5 Ma) and possibly even earlier in the Gangdese Shan. *Coleman and Hodges* [1995] interpreted the age of a mica from the hanging wall of the South Tibetan Detachment (STD) [*Burchfiel et al.*, 1992] as indicating that E-W extension was underway both there (i.e., the High Himalaya) and in the Thakkhola graben (~40 km to the NW) by ~14 Ma. This interpretation is consistent with the observations of *Yin et al.* [1994] who found that magmatism associated with N-S dike swarms (i.e., E-W extension) occurred along the Tsangpo suture zone at 15 to 18 Ma. *Yin et al.* [1994] attributed this to incipient collapse of a narrow mountain belt that was formed by thrusting within the Himalaya, Tethyan Himalaya, and southern Gangdese Shan during the late Oligocene to early Miocene [*Harrison et al.*, 1992b; *Yin et al.*, 1994]. Assuming for the moment that the extrapolation of

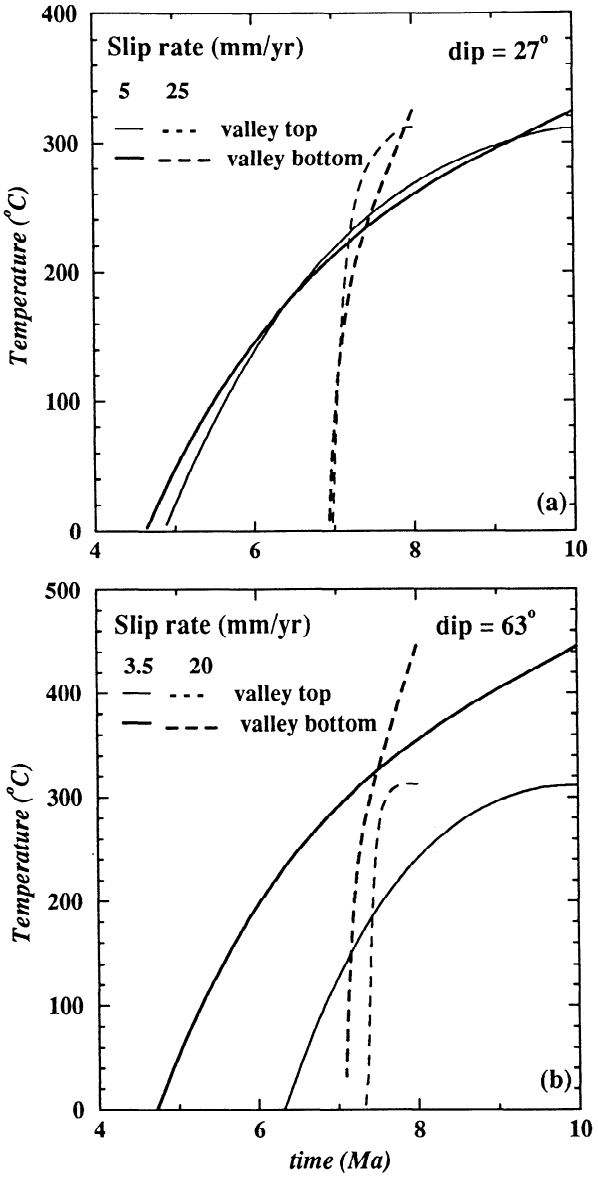

Figure 19. Calculated thermal histories appropriate to the samples from the two Nyainqentanghla traverses that result from (a) slip on a fault oriented at an angle of 27° and (b) slip on a fault oriented at 63°. For the high angle (63°) case, the samples at the top of the valley are first to cool, whether slip is rapid or slow, due to erosion at the Earth's surface. If slip occurred at low angle (~27°), the thermal histories would be the reverse of what we observe, i.e., locations closest to the fault cool prior to those at the top of the valley.

structures from the hanging wall of the STD to the Thakkhola graben [*Coleman and Hodges*, 1995] is accurate, the mechanism proposed by *Yin et al.* [1994] would seem to be the likely cause of graben formation as the Thakkhola graben clearly does not extend beyond the Tethyan Himalaya onto the Tibetan plateau (see Plate 1 of *Armijo et al.* [1986], Figure 5 of *Mercier et al.* [1987], and Figure 1 of *Rothery and Drury* [1984]). Thus the timing of initiation of the Thakkhola graben does not constrain the age at which E-W extension began within the main body of the plateau but rather reflects either a response to localized relief in the Himalaya, or to the spreading of the Himalayan arc [*Armijo et al.*, 1986]. Further complicating the above discussion is the fact that lineations associated with the STD trend systematically E-W [*Coleman*, 1993] in the region where *Coleman and Hodges* [1995] obtained their 14 Ma mica age. Thus it appears equally plausible that the dated feature is a late, steep fault related to the South Tibetan Detachment System [*Burchfiel et al.*, 1992]. If this is the case, then the 14 Ma mica age does not date the onset of N-S rifts in the central High Himalaya.

Stratigraphic and morphological evidence led *Armijo et al.* [1986] to conclude that the active, high-angle, graben-bounding normal faults on the Tibetan plateau initiated at 2.0±0.5 Ma. *Pan and Kidd* [1992] interpreted early results from the present study [*Copeland*, 1990; *Harrison et al.*, 1992b] to infer that the Nyainqentanghla ductile shear zone was active for some period between 11 and 5 Ma. Our modeling of thermal history results from the Goring-la and Balum Chun valleys indicates an initiation age of the detachment (8±1 Ma) that is consistent with but considerably more precise than these earlier assessments.

Initiation of normal faulting in the central Nyainqentanghla at 8±1 Ma is also consistent with constraints from both the northern and southern parts of the range which suggest that rapid cooling, possibly related to tectonic denudation of the range, was also occurring in those locations at that time. The master fault which makes up the eastern margin of the Nyainqentanghla splays into several smaller branches in the southern part of the range [*Armijo et al.*, 1986]. The ~100 Ma age from hornblende PC-88-44 suggests that the eastern part of this zone has not been significantly eroded relative to the region west of the master fault. The contrast between the ~8 Ma mica ages west of Damxung and the 155 Ma muscovite age for M47-7, north of Damxung, also suggests that the fault on the northern and western margin of the metamorphic rocks in the Nyainqentanghla (Figure 2a) experienced normal motion during the late Miocene.

The significance of the leucocratic vein in the Goring-la is somewhat uncertain. Because peak metamorphic temperatures are close to the inferred T_c for Pb in sphene [*Harris et al.*, 1988; *Cherniak*, 1993], we interpret the 11.2±0.2 Ma date as a minimum age for vein crystallization. Thus it appears that the foliation in the amphibolite xenolith is late Miocene or older. Whether or not this fabric is related to an early phase of motion on the detachment fault is not known. However, even if it were related, the amount of pre-8 Ma slip would have to be relatively small as metamorphic assemblages in the rocks of the Nyainqentanghla indicate that they originated at midcrustal depths of 15-20 km [*Harris et al.*, 1988], and the $^{40}Ar/^{39}Ar$ data presented here suggest that ~15 km of tectonic denudation occurred from the presently exposed shear zone subsequent to 8 Ma.

The Nyainqentanghla cooling history results may have regional tectonic significance as the rift valleys on the Tibetan plateau (Figure 1) are interpreted to be the result of gravitational collapse of the plateau following achievement of the maximum sustainable crustal thickness and elevation [e.g., *Tapponnier and Molnar*, 1976; *Molnar and Tapponnier*, 1978; *Mercier et al.*, 1987; *England and Houseman*, 1989; *Harrison et al.*, 1982b; *Molnar et al.*, 1993]. Continental crust can only be thickened so much for a given convergence rate and temperature distribution, after which a balance between thickening and gravitationally driven collapse/extrusion will be established. If the Yangbajian graben, which is part of the largest N-S rift system on the plateau, is representative of the southern Tibetan plateau in general, then the results presented here suggest that much of this region achieved a crustal thickness and elevation very near its present values by 8 Ma.

The Yangbajian graben is unusual among the rift valleys of the Tibetan plateau (Figure 1) in that it strikes NE-SW, whereas the predominant trend of these features is N6°E±8° [*Armijo et al.*, 1986]. However, extension directions within the graben are indistinguishable from the regional average of 96°E±7° [*Armijo et al.*, 1986]. The jog in the mid portion of the Yadong-Gulu rift is likely due to a preexisting lithospheric inhomogeneity [*Tapponnier et al.*, 1986]. *Searle's* [1995] statement that the Yangbajian graben is "a completely atypically structure" with respect to the Tibetan plateau rifts confuses geometry with kinematics. We concur that the orientation is unusual but again point out that extension directions in the Yangbajian graben are similar to other rift valleys studied by *Armijo et al.* [1986]. Our view is that the pertinent comparison to make among the active graben is their extension directions (kinematics) rather than the orientation of range bounding faults (geometry) which appear to be strongly influenced by preexisting structures [*Armijo et al.*, 1986]. Our principal reason for preferring the extensional collapse hypothesis over wedge extrusion is the synchroneity of the age of Nyainqentanghla detachment faulting with associated changes in cooling histories in samples from both further south in the Yadong-Gulu rift (where the graben strikes N-S) and in south-central Tibet. Thermal history data from a granodiorite (XR-2a) sampled in the Angang graben (A in Figure 1), immediately south of the Yangbajian segment of the Yadong-Gulu rift, indicate that rapid cooling possibly related to tectonic denudation began at 9±1 Ma [*Harrison et al.*, 1994; *Copeland et al.*, 1995]. Four hundred and fifty km further west (Figure 1), we have documented a similar rapid cooling event beginning at 8±1 Ma (T.M. Harrison, unpublished data, 1993) from a leucogranite porphyry (CH-30) in the footwall of the normal fault bounding the western edge of the Daga Co rift (B in Figure 1). The similarity of these two results to our estimate of initiation of the Nyainqentanghla fault at 8±1 Ma suggests that this event may have been widespread across the southern Tibetan plateau. Further such investigations of other graben on the plateau are warranted to determine if extension began everywhere at about this time or if some have very different structural histories.

At the same time as normal faulting was apparently getting underway on the plateau, the Indo-Australian oceanic lithosphere was beginning to deform. A region of deformation and anomalous seismicity south of India has been interpreted as a diffuse plate boundary that initiated at 7.5-8.0 Ma [e.g.,

Curray and Munasinghe, 1989]. We have previously suggested that onset of this unusual accommodation mechanism could have been a consequence of the increased deformational resistance gained by Tibet once it had attained maximum elevation [*Harrison et al.*, 1992b]. In this interpretation, folding and faulting of the Indo-Australian plate developed in response to the increased north-south compressional stress that resulted from plateau uplift. *Molnar et al.* [1993] subsequently assessed this force balance and concluded that an increase in the average elevation of Tibet from around 4 to 5 km would result in a change of stress from values below that needed to deform oceanic lithosphere to values that exceeded that threshold.

If the Yangbajian graben is indeed representative of the southern Tibetan plateau, then our results suggest that crustal thickness and elevation must have been close to their present values by 8±1 Ma. Since the presence of a high and large Tibetan plateau is the principal driving force for the Asian monsoon, it follows that the timing of the intensification of the monsoon also bears on plateau uplift. Carbon isotopic data from pedogenic carbonates in the Siwalik Formation in Pakistan and Nepal indicate a shift from C_3 to C_4 type vegetation in the Himalayan foothills beginning at about 7.5 Ma [*Quade et al.*, 1989; *Harrison et al.*, 1993b; J. Quade, J.M.L. Cater, T.P. Ojha, J. Adam, and T.M. Harrison, Dramatic carbon and oxygen isotopic shift in paleosols from Nepal and late Miocene environmental change across the northern Indian sub-continent, submitted to Geological Society of America Bulletin, 1995; hereinafter referred to as submitted manuscript, 1995]. *Quade et al.* [1989] proposed that this shift from forest to grassland was the result of intensification of the monsoon at about 7.5 Ma, a conjecture supported by planktonic assemblages and other indicators in Arabian Sea sediments [e.g., *Kroon et al.*, 1991]. Although *Cerling et al.* [1993] suggested that the C_3 to C_4 shift might be due to a decrease in atmospheric CO_2 alone, this now appears less likely [*Quade et al.*, submitted manuscript, 1995].

The three independent consequences of plateau uplift mentioned above, E-W extension on the Tibetan plateau, intraplate deformation of the Indo-Australia plate, and the intensification of the Asian monsoon, all point to the plateau having achieved something approaching its present extent and elevation by 8±1 Ma [*Harrison et al.*, 1992b; *Molnar et al.*, 1993]. Only after the southern Tibetan plateau reached maximum height would the first phenomena be triggered, and the remaining two would require both high elevation and possibly a larger threshold area. We have previously noted that there is ample evidence that a high but narrow (~200 km) mountain range existed from the Himalaya to the southern Gangdese Shan since the early Miocene [*Copeland et al.*, 1987, 1995; *Harrison et al.*, 1992b; *Yin et al.*, 1994] but believe it unlikely to have substantially perturbed climate beyond providing a local rain shadow. *Coleman and Hodges* [1995] recently argued that evidence of E-W extension in the High Himalaya implies that the plateau attained its high mean elevation well before late Miocene time. Their evidence for this, however, is one mica age from a fault that may not even be related to a graben that is entirely restricted to the High and Tethyan Himalaya (see Plate 1 of *Armijo et al.* [1986]). Given the well documented history of late Oligocene-early Miocene thickening in this region, extrapolation of their single result to the Tibetan plateau seems unwarranted.

The mechanisms by which the elevation of the plateau was increased to trigger these three manifestations are not well understood, in part because the existing evidence does not clearly select between a catastrophic uplift event and a more gradual increase in elevation and extent that reached an important threshold at around 8 Ma. A suggestion arising from modeling lithospheric evolution as an isoviscous continuum is that thickening leads to conditions in which a thick mantle boundary layer can be convectively thinned in a relatively brief period of time [e.g., *England and Houseman*, 1989]. The change in potential energy in the remaining lithosphere would then lead to a sudden uplift of the plateau long after the initiation of thickening. However, when similar calculations are carried out using a temperature-dependent rheology [*Buck and Toksoz*, 1983; *Lenardic and Kaula*, 1995], the mantle lithosphere resists detachment due its high strength [*Buck and Toksoz*, 1983; *Lenardic and Kaula*, 1995]. Thus it is possible that the strength of the mantle lithosphere may stabilize it against catastrophic or even gradual detachment. *Lenardic and Kaula* [1995] suggest that mantle lithosphere at the margin of the thickened region could be thermally eroded until the base of the crust is exposed to the asthenosphere. This in turn becomes a weak zone that permits the thickened mantle lithosphere to be rapidly delaminated in a manner similar to that first proposed by *Bird* [1978] producing rapid uplift. Although catastrophic mechanisms are outwardly appealing, it remains equally possible that there was no sudden uplift at ~8 Ma but rather that slow and relatively continuous crustal thickening resulted in the plateau attaining a threshold size and elevation at that time sufficient to trigger all three activities in relatively short succession. This latter view is consistent with a study of Siwalik Group sediments which suggests that a gradual floral shift began at 11 Ma and culminated in rapid expansion of C_4 grasses at ~7.5 Ma [*Quade et al.*, submitted manuscript, 1995]. Continued Neogene thickening by the distributed shortening mechanism, well documented in the Himalaya [e.g., *Le Fort*, 1989] and southern Tibet [*Yin et al.*, 1994], may alone or in conjunction with gradual lithospheric detachment be responsible for raising parts of the plateau to the elevation required to activate the two mechanical effects.

Conclusions

The $^{40}Ar/^{39}Ar$ thermochronology from samples collected along two deeply incised valleys within the Nyainqentanghla, a NE-SW trending mountain range in southern Tibet, indicates that a rapid cooling event propagated from the range core at ~8 Ma to ~4 Ma within the mylonitic shear zone that marks the eastern boundary of the massif. Estimates of both the age of initiation of detachment faulting and the slip rate history were extracted from the isotopically derived thermal histories using a finite difference model of slip on a normal fault at high angle (>40°). Results from the Goring-la and Balum Chun valleys indicate that slip began at 8±1 Ma and proceeded at an average rate of ~3 mm/yr between ~8 and 3 Ma. Numerical simulations using a variable slip angle indicate that the isotopically derived temperature histories cannot be reconciled with slip occurring at low angle (<40°). Assuming that the rift system associated with

the Nyainqentanghla fault is representative of graben on the southern Tibetan plateau, our data suggest that crustal thickness and elevation must have been close to their present values by 8±1 Ma. This is in accord with evidence that the Asian monsoon had intensified by ~7.5 Ma and, by inference, that the plateau had attained something approaching its present elevation and extent at that time. Deformation within the Indo-Australian oceanic lithosphere beginning at 7.5-8.0 Ma is also consistent with this history.

Acknowledgments. We thank Kevin Chamberlain for performing the U-Pb analyses; An Yin, Pan Yun, Li Qi (State Seismological Bureau), Barshang Tseren (Xizang Seismological Bureau), and Wang Jo for help in the field; Jeff Fillipone, Wenji Chen, and Matt Heizler for assistance with the argon isotopic analyses; Phillip England and Gordon Lister for reviewing the manuscript; and Stuart Hall for performing the paleomagnetic measurements. This research was supported by the National Science Foundation grants EAR-8721026 and EAR-9118125 and grant 49173161 from the Chinese National Natural Science Foundation.

References

Armijo, R., P. Tapponnier, J.L. Mercier, and T.-L. Han, Quaternary extension in southern Tibet: Field observations and tectonic implications, *J. Geophys. Res., 91*, 13,803-13,872, 1986.

Armijo, R., P. Tapponnier, and T.-L. Han, Late Cenozoic right-lateral strike-slip faulting in southern Tibet, *J. Geophys. Res., 94*, 2787-2838, 1989.

Baldwin, S.L., T.M. Harrison, and J.D. Fitz Gerald, Diffusion of ^{40}Ar in metamorphic hornblende, *Contrib. Mineral. Petrol., 105*, 691-703, 1990.

Bird, P., Initiation of intracontinental subduction in the Himalaya, *J. Geophys. Res., 83*, 4975-4987, 1978.

Buck, W.R., Flexural rotation of normal faults, *Tectonics, 7*, 959-973, 1988.

Buck, W.R., and M.N. Toksoz, Thermal effects of continental collision: Thickening a variable viscosity layer, *Tectonophysics, 100*, 53-69, 1983.

Burchfiel, B.C., Chen, Z., Hodges, K.V., Liu, Y., Royden, L.H., Deng, C., and Xu, J., The South Tibetan Detachment System, Himalayan Orogen: extension contemporaneous with and parallel to shortening in a collisional mountain belt, *Spec. Pap. Geol. Soc. Am., 269*, 49 pp., 1992.

Carter, N.L., and M.C. Tsenn, Flow properties of continental lithosphere, *Tectonophysics, 136*, 27-63, 1987.

Cerling, T.E., Wang, Y., and Quade, J., Global ecologic changes in the Miocene: expansion of the C_4 ecosystem, *Nature, 361*, 344-345, 1993.

Chang C. et al., Preliminary conclusions of the Royal Society - Academica Sinica 1985 geotraverse of Tibet, *Nature, 323*, 501-507, 1986.

Cherniak, D.J., Lead diffusion in titanite and preliminary results on the effects of radiation damage on Pb transport, *Chem. Geol., 110*, 177-194, 1993.

Coleman, M., West-directed extensional deformation in the North Marsyandi River region, west-central Nepal Himalaya, *Geol. Soc. Am. Abstr. Programs, 25*, A174-A175, 1993.

Coleman, M., and Hodges, K., Evidence for Tibetan plateau uplift before 14 Myr ago from a new minimum estimate for east-west extension, *Nature, 374*, 49-52, 1995.

Copeland, P., Cenozoic tectonic history of the southern Tibetan Plateau and eastern Himalaya: Evidence from $^{40}Ar/^{39}Ar$ dating, Ph.D. dissertation, 419 p., State University of New York, Albany, 1990.

Copeland, P., T.M. Harrison, W.S.F. Kidd, X. Ronghua, and Z. Yuquan, Rapid early Miocene acceleration of uplift in the Gandese Belt, Xizang-southern Tibet, and its bearing on accommodation mechanisms of the India-Asia collision, *Earth Planet. Sci. Lett., 86*, 240-252, 1987.

Copeland, P., T.M. Harrison, P. Yun, W.S.F. Kidd, and M. Roden, Thermal evolution of the Gangdese batholith, southern Tibet: A history of episodic unroofing, *Tectonics*, in press, 1995.

Coward, M.P., W.S.F. Kidd, Y. Pan, R.M. Shackelton, and H. Zhang, The structure of the 1985 Tibet geotraverse, Lhasa to Golmud, *Philos. Trans. R. Soc. London, A, 327*, 307-336, 1988.

Curray, J.R., and T. Munasinghe, Timing of intraplate deformation, northeastern Indian Ocean, *Earth Planet. Sci. Lett., 94*, 71-77, 1989.

Dewey, J.F., Extensional collapse of orogens, *Tectonics, 7*, 1123-1139, 1988.

England, P., and G. Houseman, Extension during continental convergence, with application to the Tibetan plateau, *J. Geophys. Res., 94*, 17,561-17,569, 1989.

Harris, N.B.W., T.B.J. Holland, and A.G. Tindle, Metamorphic rocks of the 1985 Tibet Geotraverse, Lhasa to Golmud, *Philos. Trans. R. Soc. London, A, 327*, 203-213, 1988.

Harrison, T.M., I. Duncan, and I. McDougall, Diffusion of ^{40}Ar in biotite: Temperature, pressure and composition effects, *Geochim. Cosmochim. Acta, 49*, 2461-2468, 1985.

Harrison, T.M., O.M. Lovera, and M.T. Heizler, $^{40}Ar/^{39}Ar$ results for alkali feldspars containing diffusion domains with differing activation energy, *Geochim. Cosmochim. Acta, 55*, 1435-1448, 1991.

Harrison, T.M., C. Wenji, P.H. Leloup, F.J. Ryerson, and P. Tapponnier, An early Miocene transition in deformation regime within the Red River fault zone, Yunnan, and its significance for Indo-Asian tectonics, *J. Geophys. Res., 97*, 7159-7182, 1992a.

Harrison, T.M., P. Copeland, W.S.F. Kidd, and A. Yin, Raising Tibet, *Science, 255*, 1663-1670, 1992b.

Harrison, T.M., M.T. Heizler, and O.M. Lovera, Implications of *in vacuo* crushing experiments to K-feldspar thermochronometry, *Earth Planet. Sci. Lett., 117*, 169-180, 1993a.

Harrison, T.M., P. Copeland, S.A. Hall,, J. Quade, S. Burner, T.P. Ojha, and W.S.F. Kidd, Isotopic preservation of Himalayan/Tibetan uplift, denudation, and climatic histories in two molasse deposits, *Jour. Geol., 101*, 159-177, 1993b.

Harrison, T.M., M.T. Heizler, O.M. Lovera, C. Wenji, and M. Grove, A chlorine disinfectant for excess argon released during step heating from K-feldspars, *Earth Planet. Sci. Lett., 123*, 95-104, 1994.

Heizler, M.T., and T.M. Harrison, The heating duration and provenance ages of rocks in the Salton Sea Geothermal Field, southern California, *J. Volcanol. Geotherm. Res., 46*, 73-97, 1991.

Jackson, J., and D. McKenzie, The geometrical evolution of normal fault systems, *J. Struct. Geol., 5*, 471-482, 1983.

Kidd, W.S.F., et al., Geological map of the geotraverse route, *Philos. Trans. R. Soc. London, A, 327*, 287-305, 1988.

Kroon, D., T. Steens, and S.R. Troelstra, Onset of the monsoonal related upwelling in the western Arabian Sea as revealed by planktonic foaminifers, edited by W.L. Prell et al., *Proc. Ocean Drill. Program, Sci. Results, 117*, 257-263, 1991.

Lenardic, A., and W.M. Kaula, More thoughts on convergent crustal plateau formation and mantle dynamics with regard to Tibet, *J. Geophys. Res.*, in press, 1995.

Le Fort, P. The Himalayan orogenic segment, edited by A.M.C. Sengör, *Tectonic Evolution of the Tethyan Region*, NATO ASI Ser. 259, pp. 289-386, Kluwer Academic, Norwell, Mass., 1989.

Lovera, O.M., F.M. Richter, and T.M. Harrison, $^{40}Ar/^{39}Ar$ geothermometry for slowly cooled samples having a distribution of diffusion domain sizes, *J. Geophys. Res., 94*, 17,917-17,935, 1989.

Lovera, O.M., F.M. Richter, and T.M. Harrison, Diffusion domains determined by ^{39}Ar released during step heating, *J. Geophys. Res., 96*, 2057-2069, 1991.

Mercier, J.-L., R. Armijo, P. Tapponnier, E. Carey-Gailhardis, and T.L. Han, Change from Tertiary compression to Quaternary extension in southern Tibet during the India-Asia collision, *Tectonics, 6*, 275-304, 1987.

Metzger, K., C.M. Raunsley, S.R. Bohlen, and G.N. Hanson, U-Pb garnet, sphene, monazite and rutile ages: Implications for the duration of high-grade metamorphism and cooling histories, Adirondack Mtns, NY, *J. Geol., 99*, 415-428, 1991.

Molnar, P. and P. Tapponnier, Active tectonics of Tibet, *J. Geophys. Res., 83*, 5361-5375, 1978.

Molnar, P., P. England, and J. Martinod, Mantle dynamics, the uplift of the Tibetan plateau, and the Indian monsoon, *Rev. Geophys., 31*, 357-396, 1993.

Naeser, C.W., The fading of fission tracks in the geologic environment - Data from deep drill holes, *Nucl. Tracks, 5*, 248-258, 1981.

Pan, Y., and W.S.F. Kidd, Nyainqentanghla shear zone: A late Miocene extensional detachment in the southern Tibetan Plateau, *Geology, 20*, 775-778, 1992.

Pan, Y., P. Copeland, M.K. Roden, W.S.F. Kidd, and T.M. Harrison, Thermal and unroofing history of the Lhasa area, southern Tibet - Evidence from apatite fission track thermochronology, *Nucl. Tracks Radiat. Meas., 21*, 543-554, 1993.

Peaceman, D.W., and H.H. Rachford, The numerical solution of parabolic and elliptic equations, *J. Soc. Ind. Appl. Math., 3*, 28-41, 1955.

Quade, J., Cerling, T.E., and Bowman, J.R., Dramatic ecologic shift in the late Miocene of northern Pakistan, and its significance to the development of the Asian Monsoon, *Nature, 342*, 163-166, 1989.

Rothery, D.A., and Drury, S.A., The neotectonics of the Tibetan Plateau, *Tectonics, 3*, 19-26, 1984.

Peltzer, G., and P. Tapponnier, Formation and

evolution of strike-slip faults, rifts, and basins during the India-Asia collision: An experimental approach, *J. Geophys. Res., 93*, 15,085-15,117, 1988.

Proffett, J.M., Cenozoic geology of the Yerington District, Nevada, and implications for the nature and origin of Basin and Range faulting, *Geol. Soc. Am. Bull., 88*, 247-266, 1977.

Richter, F.M., O.M. Lovera, T.M. Harrison, and P. Copeland, Tibetan tectonics from $^{40}Ar/^{39}Ar$ analysis of a single K-feldspar sample, *Earth Planet. Sci. Lett., 105*, 266-276, 1991.

Ruppel, C., L. Royden and K.V. Hodges, Thermal modeling of extentional tectonics: Application to pressure-temperature-time histories of metamorphic rocks, *Tectonics, 7*, 947-957, 1988.

Searle, M., The rise and fall of Tibet, *Nature, 374*, 17-18, 1995.

Tapponnier, P., and P. Molnar, Slip-line field theory and large-scale continental tectonics, *Nature, 264*, 319-324, 1976.

Tapponnier, P., G. Peltzer, and R. Armijo, On the mechanics of the collision between India and Asia, edited by M.P. Coward and A.C. Ries, *Collision Tectonics*, Geol. Soc. Spec. Publ. London, 19., 115-157, 1986.

Tapponnier, P., Mechanisms of "extensional or denudation" faulting in regions of crustal shortening: an updated review, *Late Orogenic Extension in Mountain Belts*, Abstract Volume, Éditions BRGM n° 219, 1993.

Weissel, J.K., and Karner, G.D., Flexural uplift of rift flanks due to mechanical unloading of the lithosphere during extension, *J. Geophys. Res., 94*, 13,919-13,950, 1989.

Xu, R.H., U. Schärer, and C.J. Allègre, Magmatism and metamorphism in the Lhasa block (Tibet): A geochronological study, *J. Geol., 93*, 41-57, 1985.

Yin, A., T.M. Harrison, F.J. Ryerson, W. Chen, W.S.F. Kidd, and P. Copeland, Tertiary structural evolution of the Gangdese thrust system, southeastern Tibet, *J. Geophys. Res. 99*, 18,175-18,201, 1994.

P. Copeland, Department of Geosciences, University of Houston, Houston, TX 77204.

T.M. Harrison, Department of Earth and Space Sciences, University of California, Los Angeles, CA 90024. (e-mail: tmh@argon.ess.ucla.edu)

W.S.F. Kidd, Department of Geological Sciences, State University of New York at Albany, Albany, NY 12222.

O.M. Lovera, Department of Earth and Space Sciences, University of California, Los Angeles, CA 90024.

(Received March 24, 1994;
revised October 20, 1994;
accepted November 9, 1994.)